Document made available under the Patent Cooperation Treaty (PCT)

International application number: PCT/US2004/018969

International filing date: 14 June 2004 (14.06.2004)

Document type: Certified copy of priority document

Document details: Country/Office: US
Number: 60/478,480
Filing date: 13 June 2003 (13.06.2003)

Date of receipt at the International Bureau: 01 March 2007 (01.03.2007)

Remark: Priority document submitted or transmitted to the International Bureau in compliance with Rule 17.1(a) or (b)

1577829

THE UNITED STATES OF AMERICA

TO ALL TO WHOM THESE PRESENTS SHALL COME:

UNITED STATES DEPARTMENT OF COMMERCE

United States Patent and Trademark Office

February 16, 2007

THIS IS TO CERTIFY THAT ANNEXED HERETO IS A TRUE COPY FROM THE RECORDS OF THE UNITED STATES PATENT AND TRADEMARK OFFICE OF THOSE PAPERS OF THE BELOW IDENTIFIED PATENT APPLICATION THAT MET THE REQUIREMENTS TO BE GRANTED A FILING DATE.

> **APPLICATION NUMBER: *60/478,480***
> **FILING DATE: *June 13, 2003***
> **RELATED PCT APPLICATION NUMBER: *PCT/US04/18969***

THE COUNTRY CODE AND NUMBER OF YOUR PRIORITY APPLICATION, TO BE USED FOR FILING ABROAD UNDER THE PARIS CONVENTION, IS *US60/478,480*

Certified by

Under Secretary of Commerce
for Intellectual Property
and Director of the United States
Patent and Trademark Office

PROVISIONAL APPLICATION FOR PATENT COVER SHEET

A/prov

This is a request for filing a PROVISIONAL APPLICATION FOR PATENT under 37 CFR 1.53(c).

Express Mail Label No.	EV 217411796 US

INVENTOR(S)

Given Name (first and middle [if any])	Family Name or Surname	Residence (City and either State or Foreign Country)
John	Kouvetakis	Mesa, AZ
Matthew	Bauer	Tempe, AZ
Jose	Menendez	Tempe, AZ

☑ Additional inventors are being named on the __1__ separately numbered sheets attached hereto

TITLE OF THE INVENTION (500 characters max)

DIRECT-GAP GeSn, Ge, AND SiGeSn EPILAYERS AND NANOSTRUCTURES GROWN ON SILICON

CORRESPONDENCE ADDRESS

Direct all correspondence to:

☑ Customer Number | 27887

Type Customer Number here

Place Customer Number Bar Code Label here

OR

☐ Firm or Individual Name	
Address	
Address	
City		State		ZIP	
Country		Telephone		Fax	

ENCLOSED APPLICATION PARTS (check all that apply)

☑ Specification   Number of Pages **26**

☑ Drawing(s)   Number of Sheets **5**

☐ Application Data Sheet. See 37 CFR 1.76

☐ CD(s), Number

☑ Other (specify)   **Appendices 54 pages**

METHOD OF PAYMENT OF FILING FEES FOR THIS PROVISIONAL APPLICATION FOR PATENT

☑ Applicant claims small entity status. See 37 CFR 1.27.

☑ A check or money order is enclosed to cover the filing fees

☑ The Commissioner is hereby authorized to charge filing fees or credit any overpayment to Deposit Account Number: **060590**

☐ Payment by credit card. Form PTO-2038 is attached.

FILING FEE AMOUNT ($)

$80.00

Respectfully submitted,

SIGNATURE _Richard E. Oney_

TYPED or PRINTED NAME Richard E. Oney

TELEPHONE (602) 916-5303

Date **6/13/03**

REGISTRATION NO. (if appropriate)	36,884
Docket Number:	12504.460

USE ONLY FOR FILING A PROVISIONAL APPLICATION FOR PATENT

PROVISIONAL APPLICATION COVER SHEET
Additional Page

Docket Number	12504.460

INVENTOR(S)/APPLICANT(S)		
Given Name (first and middle [if any])	Family or Surname	Residence (City and either State or Foreign Country)
Chang	Wu Hu	Gilbert, AZ
Ignatious S.	Tsong	Tempe, AZ
John	Tolle	Gilbert, AZ

Number _____2_____ of _____2_____

WARNING: Information on this form may become public. Credit card information should not be included on this form. Provide credit card information and authorization on PTO-2038.

LAW OFFICES

FENNEMORE CRAIG

A PROFESSIONAL CORPORATION

RICHARD E. ONEY
Direct Phone: (602) 916-5303
Direct Fax: (602) 916-5503
roney@fclaw.com

OFFICES IN:
PHOENIX, TUCSON AND NOGALES

3003 NORTH CENTRAL AVENUE
SUITE 2600
PHOENIX, ARIZONA 85012-2913
PHONE: (602) 916-5000
FAX: (602) 916-5999

June 13, 2003

VIA EXPRESS MAIL – EV 217411796 US

MS Provisional Patent Application
Commissioner for Patents
P.O. Box 1450
Alexandria, VA 22313-1450

      Re: Submission of a New United States Provisional Patent Application
              Title: DIRECT-GAP GeSn, Ge, AND SiGeSn EPILAYERS AND
              NANOSTRUCTURES GROWN ON SILICON
              Inventors: Kouvetakis, et al.
              Filing Date: June 13, 2003
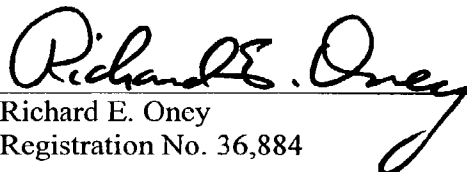   Our Ref No.: 12504.460

Dear Sir:

        We hereby submit the following documents concerning the referenced patent application:

1. Fee Transmittal Form for FY 2003 (PTO/SB/17);
2. Provisional Application for Patent Cover Sheet (PTO/SB/16);
3. Provisional Patent Application, including a specification (26 pages), drawing figures (5 pages), and appendices (54 pages);
4. Check for $ 80.00 to cover the filing fee; and
5. Postage-paid postcard acknowledging receipt of this letter and the foregoing.

        Please accord this application a serial number and a filing date. Applicant claims small entity status. The Commissioner is hereby authorized to charge any additional fee required or credit any overpayments to Deposit Account No. 060590.

                      Respectfully submitted,

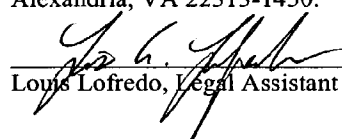   By   Richard E. Oney
                          Richard E. Oney
                          Registration No. 36,884

FENNEMORE CRAIG

Express Mail Label No. EV 217411796 US   Date of Deposit _6/13/03_

I hereby certify that this paper and all documents and any fee referred to herein are being deposited on the date indicated above with the U.S. Postal Service "Express Mail Post Office to Addressee" service under 37 C.F.R. § 1.10, and is addressed to MS Provisional Patent Application, Commissioner for Patents, P.O. Box 1450, Alexandria, VA 22313-1450.

_6/13/03_

Louis Lofredo, Legal Assistant   Date of Signature

FEE TRANSMITTAL
for FY 2003
Effective 01/01/2003. Patent fees are subject to annual revision.

[X] Applicant claims small entity status. See 37 CFR 1.27

TOTAL AMOUNT OF PAYMENT ($) 80

Complete if Known

Application Number	Unassigned
Filing Date	June 13, 2003
First Named Inventor	Kouvetakis, et al.
Examiner Name	Unassigned
Art Unit	Unassigned
Attorney Docket No.	12504.460

METHOD OF PAYMENT (check all that apply)

[X] Check [ ] Credit card [ ] Money Order [ ] Other [ ] None

[X] Deposit Account:

Deposit Account Number: 060590

Deposit Account Name: Fennemore Craig, P.C.

The Commissioner is authorized to: (check all that apply)

[ ] Charge fee(s) indicated below   [X] Credit any overpayments

[X] Charge any additional fee(s) during the pendency of this application

[ ] Charge fee(s) indicated below, **except for the filing fee**
to the above-identified deposit account.

FEE CALCULATION

1. BASIC FILING FEE

Large Entity Fee Code	Fee ($)	Small Entity Fee Code	Fee ($)	Fee Description	Fee Paid
1001	750	2001	375	Utility filing fee	
1002	330	2002	165	Design filing fee	
1003	520	2003	260	Plant filing fee	
1004	750	2004	375	Reissue filing fee	
1005	160	2005	80	Provisional filing fee	80

SUBTOTAL (1) ($) 80

2. EXTRA CLAIM FEES FOR UTILITY AND REISSUE

	Extra Claims		Fee from below	Fee Paid
Total Claims	-20** =	X	9	= 0
Independent Claims	-3** =	X	42	= 0
Multiple Dependent				=

Large Entity Fee Code	Fee ($)	Small Entity Fee Code	Fee ($)	Fee Description
1202	18	2202	9	Claims in excess of 20
1201	84	2201	42	Independent claims in excess of 3
1203	280	2203	140	Multiple dependent claim, if not paid
1204	84	2204	42	** Reissue independent claims over original patent
1205	18	2205	9	** Reissue claims in excess of 20 and over original patent

SUBTOTAL (2) ($) 0

**or number previously paid, if greater; For Reissues, see above*

FEE CALCULATION (continued)

3. ADDITIONAL FEES

Large Entity Fee Code	Fee ($)	Small Entity Fee Code	Fee ($)	Fee Description	Fee Paid
1051	130	2051	65	Surcharge - late filing fee or oath	
1052	50	2052	25	Surcharge - late provisional filing fee or cover sheet	
1053	130	1053	130	Non-English specification	
1812	2,520	1812	2,520	For filing a request for *ex parte* reexamination	
1804	920*	1804	920*	Requesting publication of SIR prior to Examiner action	
1805	1,840*	1805	1,840*	Requesting publication of SIR after Examiner action	
1251	110	2251	55	Extension for reply within first month	
1252	410	2252	205	Extension for reply within second month	
1253	930	2253	465	Extension for reply within third month	
1254	1,450	2254	725	Extension for reply within fourth month	
1255	1,970	2255	985	Extension for reply within fifth month	
1401	320	2401	160	Notice of Appeal	
1402	320	2402	160	Filing a brief in support of an appeal	
1403	280	2403	140	Request for oral hearing	
1451	1,510	1451	1,510	Petition to institute a public use proceeding	
1452	110	2452	55	Petition to revive - unavoidable	
1453	1,300	2453	650	Petition to revive - unintentional	
1501	1,300	2501	650	Utility issue fee (or reissue)	
1502	470	2502	235	Design issue fee	
1503	630	2503	315	Plant issue fee	
1460	130	1460	130	Petitions to the Commissioner	
1807	50	1807	50	Processing fee under 37 CFR 1.17(q)	
1806	180	1806	180	Submission of Information Disclosure Stmt	
8021	40	8021	40	Recording each patent assignment per property (times number of properties)	
1809	750	2809	375	Filing a submission after final rejection (37 CFR 1.129(a))	
1810	750	2810	375	For each additional invention to be examined (37 CFR 1.129(b))	
1801	750	2801	375	Request for Continued Examination (RCE)	
1802	900	1802	900	Request for expedited examination of a design application	

Other fee (specify) _____

*Reduced by Basic Filing Fee Paid

SUBTOTAL (3) ($) 0

SUBMITTED BY

(Complete *if applicable*)

Name (Print/Type)	Richard E. Oney	Registration No. (Attorney/Agent)	36,884	Telephone	602 916-5303
Signature	*Richard E. Oney*			Date	June 13, 2003

U.S. PROVISIONAL PATENT APPLICATION FOR

DIRECT-GAP GeSn, Ge, AND SiGeSn EPILAYERS AND NANOSTRUCTURES GROWN ON SILICON

Inventors: John Kouvetakis
7032 E. Indigo
Mesa, Arizona 85207

Matthew Bauer
1996 E. Rice Drive
Tempe, Arizona 85283

Jose Menendez
309 E. 14th Street
Tempe, Arizona 85281

Chang Wu Hu
1688 W Encinas St
Gilbert, Arizona 85233

Ignatious S. Tsong
1445 E. Palomino Drive
Tempe, Arizona 85284

John Tolle
1489 S. Dove St.
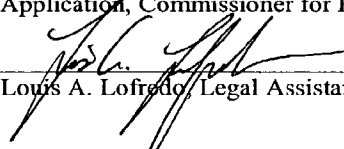Gilbert, Arizona 85233

Assignee: The Arizona Board of Regents, Acting for and on behalf of the Arizona State
University
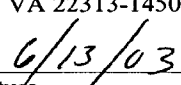
Attorney Ref. No.: 12504.460

Express Mail Label No. EV217411796US   Date of Deposit June 13, 2003

I hereby certify that this paper is being deposited with the U.S. Postal Service "Express Mail Post Office to
Addressee" service under 37 CFR 1.10 on the date indicated above and addressed to MS Provisional Patent
Application, Commissioner for Patents, P.O. Box 1450, Alexandria, VA 22313-1450.

_____   _____6/13/03_____
Louis A. Lofredo/Legal Assistant   Date of Signature

DIRECT-GAP GeSn, Ge AND SiGeSn EPILAYERS AND NANOSTRUCTURES GROWN ON SILICON

STATEMENT OF GOVERNMENT FUNDING

BACKGROUND OF THE INVENTION

[0002] This invention relates generally to semiconductor materials and, more particularly, to semiconductor structures having direct-gap GeSn, Ge and SiGeSn epilayers and nanostructures formed on silicon.

[0003] It has been known for many years—on theoretical grounds—that the Sn-Ge alloy system and the Si-Ge-Sn ternary alloy should have very interesting properties, especially as infrared devices. This has stimulated intense experimental efforts to grow such compounds, but for many years the resulting material quality has been incompatible with device applications.

[0004] The physical properties of most semiconductor alloys are smooth functions of their composition, providing a very versatile tool for device engineering. Alloys of elemental semiconductors such as Si and Ge, and alloys of III-V compounds such GaAs, AlAs, InAs, and InP, play a key role in high-speed microelectronics[1] and in optoelectronics.[2] In particular, the group-IV Ge_xSi_{1-x} system is a nearly ideal semiconductor alloy, with a lattice constant and interband optical transition energies that are essentially linear functions of x.[3]

[0005] An even more intriguing group-IV alloy is the $Ge_{1-x}Sn_x$ system. Group-IV semiconductors are notorious for not displaying a direct band gap, which precludes their use as active layers in light-emitting diodes and lasers. The band gap of the $Ge_{1-x}Sn_x$ alloy, however, is expected to undergo an indirect-to-direct transition, since the direct band gap has a value of 0.81 eV in Ge and becomes negative (-0.4 eV) in gray (α-) Sn.[4] A linear interpolation between Ge and α-Sn places the crossover at $x = 0.2$, and this simple estimate agrees remarkably well with detailed electronic structure calculations within the virtual crystal approximation.[5,6]

[0006]   Unfortunately, the growth of $Ge_{1-x}Sn_x$ alloys has been hampered by the enormous lattice mismatch (15%) between Ge and α-Sn and the instability of the cubic α-Sn structure above 13°C. As a result, the system is highly metastable and cannot be produced in bulk form. However, the reported stabilization of α-Sn in films grown by molecular beam epitaxy (MBE) on InSb and CdTe substrates[7] encouraged several groups to attempt the growth of $Ge_{1-x}Sn_x$ using the same procedure. Significant progress has been made,[8,9] but the large compositional dependence of the lattice constant limits this approach to a narrow range of compositions near the Sn-rich end. For the Ge-rich $Ge_{1-x}Sn_x$ alloys, which are of more interest technologically, pure Ge is an obvious choice as a substrate, and in fact fully strained Sn_nGe_m superlattices[10] as well as random $Ge_{1-x}Sn_x$ alloys[11] on Ge have been demonstrated. Unfortunately, a major disadvantage of Ge substrates is that tetragonally distorted $Ge_{1-x}Sn_x$ films on Ge are not expected to display an indirect-to-direct transition. Ge-rich Sn_xGe_{1-x} films have been grown by Pukite, Harwit, and Iyer[12] and by He and Atwater[13]on Si substrates using Ge buffer layers. The optical properties of these films, however, differ very markedly[13] from those observed in conventional semiconductor alloys: individual interband transitions are not observed, and the position of the band edges is obtained from fits that must incorporate transitions not found in pure Ge.

[0007]   The unusual optical properties of Sn_xGe_{1-x} alloys[13] suggest that it may not be possible to describe the $Ge_{1-x}Sn_x$ system in terms of an effective band structure, as is usually done with well-behaved semiconductor alloys. An anomalous dependence of the physical properties on composition has in fact been predicted for alloys of very different materials, such as GaAsN,[14] and given the large mismatch between Ge and Sn, similar findings would not be entirely surprising for $Ge_{1-x}Sn_x$ alloys. If this were the case, the possible applications of Sn_xGe_{1-x} alloys would be severely limited.

SUMMARY OF THE INVENTION

[0008]   According to the present invention, there is provided a novel method for synthesizing device-quality alloys and ordered phases in a Si-Ge-Sn system using a UHV-CVD process. The method is based on precursor CVD in which growth mechanisms and surface kinetics are substantially different than those inherent to MBE processes to generate new materials (epilayers and nanostructures) that cannot be created by conventional CVD and MBE

routes. The range of target materials is wide. In this document we focus on specific systems that are likely to be used in fabrication of new and efficient infrared photodetectors and sensors as described below.

[0009] In accordance with the invention, we have grown device-quality Sn-Ge and Sn-Ge-Si materials directly on Si substrates. We have determined the optical properties of strain-free $Ge_{1-x}Sn_x$ films grown directly on Si. Unlike previous results, our films show clear evidence for a well-defined Ge-like band structure, demonstrating that $Ge_{1-x}Sn_x$ alloys are viable candidates for a variety of novel devices based solely on group-IV materials. Thus, the method of our invention can be used to fabricate novel Si-Ge-Sn semiconductors materials with tunable band gaps, which are suitable for highly sensitive IR photodetectors (1.55- 2.2 μm)

[0010] Semiconductor structures according to the invention include $Ge_{1-x}Sn_x$ alloys (x = 0.02-0.15) that exhibit adjustable direct bandgaps between 0.7 eV and 0.4 eV, novel ordered structures with composition Ge_5Sn, strained direct gap Ge layers grown on $Sn_{1-x}Ge_x$ buffer layers, ternary $(SiGe)_{1-x}Sn_x$ solid solutions as well as related multilayer $Si/Ge_{1-x}Sn_x/Ge$ heterostructures that are easy to manufacture and are predicted to exhibit intense absorption at 1.55 μm. The optical properties indicate that these materials can be used to fabricate new and efficient infrared photodetectors and sensors and related optical communication devices.

[0011] Semiconductor nanostructures such as Ge-Sn and Si-Ge-Sn quantum dots with tunable electronic and structural properties and nanowires of Ge-C alloys can be formed directly on silicon substrates. Si-Ge-Sn nanostructures with direct tunable bandgaps combined with the underlying Si substrate should have tremendous potential for use in infrared laser technologies, which makes them more desirable than any device based on Si and Ge.

BRIEF DESCRIPTION OF THE DRAWINGS AND APPENDICES

[0012] The accompanying drawings, which are incorporated in and constitute a part of the specification, illustrate the presently preferred embodiments of the invention. Together with the general description given above and the detailed description of the preferred embodiments and methods given below, they serve to explain the principles of the invention.

4

[0013] FIGs. 1A and 1B show Rutherford backscattering spectra of two representative SnGe/Si films according to the present invention demonstrating full Sn substitutionality.

[0014] FIG. 1C shows a high-resolution electron micrograph of the interface region of a representative SnGe/Si film according to the invention, with arrows showing misfit dislocations.

[0015] FIG. 1D is an electron micrograph showing the film surface of a representative SnGe/Si film according to the invention.

[0016] FIG. 1E shows a selected-area diffraction pattern of a representative SnGe/Si film according to the invention.

[0017] FIG. 2 is a graph of the absorption coefficients of bulk Ge and of a $Sn_{0.02}Ge_{0.98}$ alloy grown on Si according to the invention, which shows the order-of-magnitude increase of absorption at 1.55 μm.

[0018] FIG. 3 is a graph of the second derviative of the dielectric function from ellipsometric measurements, in which the direct bandgap for $Sn_{0.02}Ge_{0.98}$ and $Sn_{0.14}Ge_{0.86}$ are 0.74 eV and 0.41 eV, respectively, are compared to 0.81 eV for Ge.

[0019] FIG. 4 is a graph of the second derivative of the imaginary part of the dielectric function near the E_1 transition, which shows that the E_1 for $Sn_{0.02}Ge_{0.98}$ and $Sn_{0.14}Ge_{0.86}$ are 2.07 eV and 1.78 eV respectively, compared to 2.12 eV for Ge.

[0020] FIG. 5 is a band diagram of pure Ge. The red line and arrows show schematically the redshift in bandgap energies for E_0(direct gap), E_1, $E_1+\Delta E_1$, E_2 etc. with incorporation of Sn into Ge.

[0021] FIGs. 6A-6C show band gap energies vs. Sn concentration x for $Ge_{1-x}Sn_x$ (x=2-20 %) and depict a systematic reduction of the gap energies with increasing Sn content. FIG. 6A shows E_1 and $E_1+\Delta_1$. FIG. 6B shows E_2. FIG. 6C shows the E_0' critical points of the band structure.

[0022] FIG. 7 shows the predicted band gaps of tensile-strained Ge as a function of the Sn concentration in the Sn_xGe_{1-x} buffer layer.

[0023]   FIG. 8 is an XTEM micrograph of the entire Si/Sn-Ge/Ge heterostructure thickness showing virtually no defects terminating at the top surface. Plan view TEM analysis shows that the defects are mainly concentrated at the Ge-Sn buffer layer.

[0024]   FIG. 9 is a low energy SIMS elemental profile of $Ge_{1-x}Sn_x (As)_y$ grown by reactions of $As(GeH_3)_3$ with digermane and SnD_4 showing a highly uniform As concentration throughout the sample. The As incorporation is readily increased by raising the partial pressure of $As(GeH_3)_3$ in the reaction mixture. Superdoped single-crystalline films with As concentration up to 2 at.% have been prepared using this new method.

[0025]   FIG. 10 shows the conduction band offset for a Ge/SiGeSn heterostructure at constant strain. The lower curve shows the Si concentration needed to keep the strain constant as the Sn concentration is increased.

[0026]   FIG. 11 shows RBS random (black trace) and aligned (red trace) spectra of $Ge_{0.82}Si_{0.13}Sn_{0.05}$ grown on $Ge_{0.95}Sn_{0.05}/Si(100)$. The channeling for Si, Sn and Ge is the same indicating single phase material.

[0027]   FIG. 12 shows a 1.55μm IR photodetector based on simple Ge/Sn-Ge herostructures.

[0028]   FIG. 13 is an XTEM micrograph of the $Ge_{4-5}Sn$ sample demonstrating that the ordered phase forms adjacent to the Si(111) inteface throughout the layer. The inset image is the diffraction pattern of the entire layer and the Si substrate, which shows a clear set of superlattice spots corresponding to the ordering along the (111) direction.

[0029]   FIG. 14 depicts models of the layered Ge_5Sn alloys consistent with the Z-contrast atomic resolution microscopy.

[0030]   FIG. 15 is a sequence of LEEM frame-captured images from an 8-μm diameter area of GeSn growth showing layer-by-layer growth. The thickness of the GeSn epitaxial layer is indicated below each image.

[0031]   FIG. 16A is an XTEM image of a $Ge_{1-x}Sn_x$ (x=0.03) island on Si(100), showing a small quantum dot exhibiting highly coherent epitaxial and defect-free character. The micrograph illustrates the relationship between size and quality of epitaxial growth.

6

[0032]   FIG. 16B is an XTEM image of another $Ge_{1-x}Sn_x$ (x=0.03) island on Si(100), showing a larger island in which strain is relieved via formation of (111) stacking faults.

[0033]   FIG. 17A is a high resolution XTEM image of periodic arrays of highly coherent and stoichiometric SiGe islands grown on Si(100) with uniform size distribution at 450°C.

[0034]   FIG. 17B is an XTEM image of a $Si_{0.50}Ge_{0.50}$ island grown at 600°C.

[0035]   FIG. 17C is an XTEM image of a $Si_{0.50}Ge_{0.50}$ island grown at 700°C.

[0036]   FIG. 18A is a high resolution XTEM image of a Si-Ge-Sn island on Si.

[0037]   FIG. 18B is an island-Si interface showing perfect epitaxy.

[0038]   FIG. 18C is a SEM image of an island ensemble.

[0039]   FIG. 18D is a plan-view XTEM image showing Moire fringes of two Si-Ge-Sn islands and the Si substrate.

[0040]   FIG. 19 shows a schematic representation of the $A(BH_3)_4$ cluster where {A,B} = {Si,Ge,Sn}, with the dark gray sphere representing A, the light gray spheres representing B, and the white spheres representing H.

[0041]   FIG. 20A shows XTEM images and EELS profiles of Si_4Ge islands grown on Si(100) at 450° C.

[0042]   FIG. 20B shows periodic anays of islands with fairly uniform size distribution line across island indicates EELS line scan.

[0043]   FIG. 20C is an EELS profile showing a uniform 20% Ge content across an island with a typical island height of 50 nm.

[0044]   FIG. 21 shows an XTEM image of a $Ge_{0.91}C_{0.09}$ island grown on the surface of Ge-C layer, with an inset atomic force microscopy (AFM) image showing an ensemble of islands on Ge-C surface.

[0045]   FIG. 22 shows Ge-C nanowires grown on a $Ge_{1-x}C_x$ epilayer (x ~ 13 at. %) on Si(001) substrate grown with $CH_2(GeH_3)_2$ precursor at 540° C.

[0046]   The following appendices, which are included as part of this application, are incorporated by this reference.

[0047] Appendix A[16] is an article entitled "Ge-Sn Semiconductors for Band-gap and Lattice Engineering" [M. Bauer, J. Taraci, J. Tolle, A. V. G. Chizmeshya, S.Zollner, D. J. Smith, J. Menendez, C. Hu, and J. Kouvetakis, App. Phys. Lett. **81**, 2992 (2002)], which describes the growth of $Ge_{1-x}Sn_x$ alloys directly on Si(100) which exhibit high thermal stability, superior crystallinity, and crystallographic and optical properties.

[0048] Appendix B[18] is an article entitled "Tunable Band Structures in Diamond-cubic Tin-Germanium Alloys Grown on Silicon Substrates" [M. Bauer, J. Tolle, C. Bungay, A.V.G. Chizmeshya. D.J. Smith, Jose Menendez, and J. Kouvetakis], which describes the growth of Sn_xGe_{1-x} alloys directly on silicon using methods based on deuterium-stabilized Sn hydrides.

[0049] Appendix C[22] is an article entitled "Synthesis of Ternary SiGeSn Semiconductors on Si(100) via Sn_xGe_{1-x} Buffer Layers" [Matthew Bauer, A.V.G. Chizmeshya. D.J. Smith, Jose Menendez, and J. Kouvetakis], which describes $Si_{1-x-y}Ge_xSn_y$ alloys grown on Si(100) facilitated by $Ge_{1-x}Sn_x$ buffer layers.

[0050] Appendix D is an article entitled "New and Practical Procedures for Development of $Ge_{1-x-y}Sn_xE_y$ (E=P, As, Sb) and Related Semiconductor Alloys", which describes novel methods and compounds for incorporating group V atoms such as P, As and Sb into Ge-Sn materials and other group IV semiconductors as well as synthesis of superconductive Si-Ge: P, As, Sb.

DESCRIPTION

SiGeSn semiconductor epilayers for IR sensors

CVD growth of $Ge_{1-x}Sn_x$ (x=2-20%) directly on Si(100)

[0051] We recently demonstrated the growth of strain-free, device-quality Sn_xGe_{1-x} films directly on Si substrates using a specially developed CVD method.[15-18] The standard CVD sources for the growth of Si and Ge are SiH_4 and GeH_4, respectively. SnH_4 is therefore the obvious choice as a Sn source, but this compound is unstable at room temperature and therefore unsuitable as a CVD precursor. However, we discovered that SnD_4 combined with high-purity H_2 (15-20% by volume) remains stable at 22°C for extended time periods, and we use this compound as our CVD Sn source. The growth proceeds at remarkably low temperatures, between 250°C and 350°C, which makes it possible to grow thick films (50-500 nm) with Sn concentrations up to 20%. The material is strain-free, with lattice parameters that

are adjustable between 5.772 Å and 5.833 Å. The lattice mismatch between the Sn_xGe_{1-x} layers and the Si substrate is accommodated by the formation of periodic Lomer edge dislocations which are parallel to the interface plane and do not degrade the crystallinity and properties of the film. Typical cross-sectional transmission electron microscopy (XTEM) and Rutherford backscattering (RBS) spectra demonstrating high quality Ge-Sn growth on Si(100) are shown in FIGs. 1A-1D. Our method invariably produces films with high uniformity that possess remarkably smooth surface morphologies (typical AFM rms values are 0.5 and 1.4 nm) and extremely low densities of threading defects, particularly for Sn concentrations between 2% and 6%. These results are unexpected (the quality of pure Ge films of Si grown by similar methods is much worse) and very intriguing, because Sn_xGe_{1-x} alloys have been predicted to become direct-gap semiconductors for concentrations near $x = 0.2$.[5,6]

Optical properties

[0052] The optical properties of Sn_xGe_{1-x} films grown on Si substrates according to our invention were studied using spectroscopic ellipsometry. Measurements in the infrared were performed using a Fourier-Transform Infrared Spectroscopy (FTIR) ellipsometer available from J.A. Woollam, Co. of Lincoln, Nebraska. Measurements in the visible range also have been performed. FIG. 2 is a graph of the absorption coefficients of bulk Ge and of a $Sn_{0.02}Ge_{0.98}$ alloy grown on Si. As shown in FIG. 2, the addition of a very small Sn fraction increases by an order of magnitude the absorption coefficient at the 1.55 µm wavelength. Because this wavelength is typically used for fiber optic communications, this demonstrates the potential of Sn_xGe_{1-x} alloy for use in high-efficiency infrared detectors.

[0053] By computing derivatives of the optical constants as a function of the photon energy, one can determine the energies of critical points in the electronic structure, in particular the direct band gap E_0 which determines the sharp increase in absorption shown in FIG. 2. FIG. 3 shows the second derivative of the imaginary part of the dielectric function for two samples of Sn_xGe_{1-x} films according to the invention. The sharp feature shown in FIG. 3 is associated with the direct band gap E_0, which can be determined with a precision of 10 meV. The direct gap is $E_0 = 0.41$ eV for $Sn_{0.14}Ge_{0.86}$. Comparing with $E_0 = 0.81$ eV for Ge, we find a dramatic band gap reduction of 50% for only 14% Sn.

[0054] FIG. 4 shows ellipsometric results near the E_1 and $E_1+\Delta_1$ transitions between the highest valence bands and the lowest conduction band at the L-point of the fcc Brillouin zone (see FIG. 5). The shape of the curve is very similar to that obtained for pure Ge, confirming the high quality of our films. From these data one can also determine the relevant optical transitions with high accuracy.

[0055] Since our films grow essentially strain-free, there is in principle no upper limit to the Sn concentration that can be achieved. Thus, our approach represents the most straightforward route to direct-gap Sn_xGe_{1-x} alloys and a practical solution to the long-standing problem of growing direct-gap semiconductors on Si. The very large lattice mismatch between our films and the Si substrate opens up intriguing new opportunities for band gap and strain engineering on silicon, as discussed below.

Mapping of the compositional and temperature dependence of the band structure of Sn_xGe_{1-x} alloys

[0056] Our results for the E_0 as well as the E_1 and $E_1+\Delta_1$ transitions show very large deviations from a simple linear interpolation of transition energies between Ge and α-Sn. Thus the determination of the compositional dependence of the band structure on Sn concentration is critical for the design of devices based on Sn_xGe_{1-x}. We are conducting systematic ellipsometric studies as a function of composition in the IR range using infrared ellipsometry. Since the lowest direct band gap of these compounds is small, its temperature dependence may be important for device design and will be studied in detail.

[0057] We have recently obtained additional spectroscopic ellipsometry data in the visible spectral range for samples across the compositional range of 2 and 20 % Sn. The results indicate the existence of a well-defined band structure similar to Ge, as expected for highly crystalline films. We were able to obtain accurate values for the E_1, $E_1+\Delta_1$, E_2 and E_0' critical points, which showed that the corresponding gap values decrease monotonically with increasing Sn concentration in the films (FIG. 6). FIGs. 6A-6C show band gap energies vs. Sn concentration x for $Ge_{1-x}Sn_x$ (x=2-20 %) and depict a systematic reduction of the gap energies with increasing Sn content. FIG. 6A shows E_1 and $E_1+\Delta_1$. FIG. 6B shows E_2. FIG. 6C shows the E_0' critical points of the band structure. Collectively, the data in FIGs. 2-6 indicate that Sn incorporation into Ge lattice sites dramatically increases the sensitivity of this system to infrared

radiation. Thus, the new alloys according to our invention are excellent candidates for a new generation of IR photodetectors, with the important additional benefit that they can be grown on inexpensive Si substrates.

Strained Ge on Sn_xGe_{1-x} buffer layers

[0058]   FIG. 7 shows a calculation of the direct and indirect edges of Ge strained to lattice-match a Sn_xGe_{1-x} buffer layer as a function of the Sn concentration in the Sn_xGe_{1-x} buffer layer. The calculation is based on deformation potential theory, and it shows a very interesting feature: strained Ge becomes a direct gap material if the Sn concentration in the buffer layer exceeds 11%. This was recognized by Soref and Friedman almost 10 years ago,[19] and they proposed several heterostructures for *p-i-n* injection lasers.

[0059]   We have recently succeeded in growing nearly defect-free Ge films on Sn_xGe_{1-x} buffer layers in accordance with the invention. A complete characterization of the strain properties indicates that the Ge films are tensile strained as expected for a material grown on a surface that possesses a larger lattice dimension. In a typical experiment the growth of Sn_xGe_{1-x} is conducted by reaction of the appropriate combinations of SnD_4 and Ge_2H_6 in an ultra-high vacuum (UHV) CVD chamber. The Ge overlayers are deposited at 400-450°C by thermally activated dehydrogenation of Ge_2H_6 on Ge-Sn buffer layers, which have typical thickness of 20-200 nm. Cross-sectional electron micrographs show completely epitaxial Ge grown on $Ge_{0.97}Sn_{0.03}$ FIG. 8 is an XTEM micrograph of the entire Si/Sn-Ge/Ge heterostructure thickness. The Ge layer is free of stacking and threading defects. Virtually all of the defects are concentrated at the Ge-Sn buffer layer, and the Ge overlayer in the upper portion of the heterostructure remains virtually defect-free (see FIG. 8).

[0060]   We plan a systematic investigation of these layers, including x-ray/RBS experiments to measure the epitaxial strain and FTIR-ellipsometry measurements to verify the predictions in FIG. 7. Both the direct and indirect gaps are expected to be lower than those of pure Ge. Furthermore, since the direct gap drops faster than the indirect gap, strained Ge materials grown on Ge-Sn buffer layers are expected to be a more sensitive photodetector than normal Ge.

11

Doping of Sn$_x$Ge$_{1-x}$ alloys and the direct-indirect crossover

[0061]   The decrease of the E_0 energy determined experimentally as a function of composition in Sn$_x$Ge$_{1-x}$ alloys is much larger than theoretically predicted.[4,5] This suggests that the direct-indirect crossover may have occurred in some of our samples, even though their Sn concentration is less than 20%. Because ellipsometry is not very sensitive to indirect transitions, we have not been able to measure the lowest indirect gap. Photoluminescence measurements are not conclusive given the possible proximity of the direct and indirect edges and the likely borrowing of intensity due to alloy mixing. We believe that the most conclusive proof of an indirect-direct crossover would be a measurement of the effective mass m^* of carriers in n-type material. The experiment consists in determining the carrier concentration n from Hall measurements and simultaneously determining the plasma oscillation frequencies from FTIR-ellipsometry measurements. The plasma frequency is given by[20]

[0062] $$\omega_p^2 = \frac{4\pi n e^2}{m^*},$$

where e is the electron charge, so that the effective mass can be calculated if the carrier concentration is known. These measurements should be very sensitive to the direct-indirect crossover because the effective mass of carriers at the Γ-point of the Brillouin zone should be much smaller than the effective mass of carriers located at the L-point valleys.

[0063]   The need to carry out these experiments and the need for doped layers in the proposed Sn$_x$Ge$_{1-x}$ devices indicate that finding a way to dope our Sn$_x$Ge$_{1-x}$ alloys is important. Currently, Si and SiGe are doped with B using diborane, and with As by implantation methods, but there are limits to how much dopant can be incorporated into the structure. In the case of As we propose to increase the free carrier concentration by building precursors with direct Ge-As bonds such as As(GeH$_3$)$_3$. We recently synthesized this compound as well as the Sb(GeH$_3$)$_3$ and P(GeH$_3$)$_3$ analogs by using a new approach that affords high yields which are viable for application in semiconductor device development. These compounds have the necessary stability and vapor pressure to be used as reactants during growth of Sn$_x$Ge$_{1-x}$. The Sb(GeH$_3$)$_3$ and P(GeH$_3$)$_3$ analogs are utilized to dope Sn$_x$Ge$_{1-x}$ with antimony and phosphorus, respectively. We use Secondary Ion Mass Spectrometry depth profile analysis (SIMS) to determine the As(Sb,P) elemental distribution and Hall/FTIR ellipsometry measurements to determine carrier concentrations and effective masses. Initial deposition studies have shown that

As is readily incorporated into the Ge-Sn lattice. The As levels are controlled by the partial pressure of the $As(GeH_3)_3$ vapor in the reaction mixture. Low energy SIMS was used to examine the elemental profile in the films. FIG. 9 is a low energy SIMS elemental profile of $Ge_{1-x}Sn_x (As)_y$ grown by reactions of $As(GeH_3)_3$ with digermane and SnD_4 showing a highly uniform As concentration throughout the sample. The As incorporation is readily increased by raising the partial pressure of $As(GeH_3)_3$ in the reaction mixture. Superdoped single-crystalline films with As concentration up to 2 at.% have been prepared using this new method. High resolution XTEM and RBS data indicated good crystal quality. Since the band gap is vanishing in Ge-Sn with increasing Sn concentration, one might be able to dope this material (through incorporation of group V (P,As,Sb) atoms into the molecular precursors) so as to increase the density of states and produce a true covalent metal or semimetal. Covalent semimetals or metals, such as the recently discovered superconducting magnesium diboride, are very rare. The potential to open up new classes of similar covalent systems through CVD techniques is of interest. The atomic constituents of these Ge-Sn:As(Sb) materials might assume alternative structural arrangements (exotic polymorphic phases) with novel elastic and electronic properties.

Ternary SnGeSi alloys

[0064]   There is in principle no reason why our CVD technique cannot be extended to the growth of ternary SnGeSi alloys. The expected properties of this system are very intriguing, as discussed theoretically by Soref and Perry.[21] Since no experimental data is available, these authors computed the properties of SnGeSi alloys using a linear interpolation scheme. Following this approach—combined with deformation potential theory—we have theoretically analyzed strained Ge layers grown on relaxed SnGeSi alloys. The most remarkable finding, which highlights the importance of growing this system, is that the Ge/SnGeSi heterostructure is a direct gap Type I system (both electrons and holes confined in the strained Ge layers) for appropriately selected Si/Sn ratios. This is illustrated in FIG. 10, which shows the conduction band offset for a Ge/SiGeSn heterostructure at constant strain. The lower curve shows the Si concentration needed to keep the strain constant as the Sn concentration is increased. The first data point corresponds to a Sn concentration for which the band gap of Ge is direct (due to strain), with the conduction band minimum at the Γ point $3k_BT$ below the conduction band minimum at the L point. Then the Si concentration and Sn concentrations are

13

increased in such a way that the strain in the pure Ge layer is the same. We see that for x(Sn) > 0.23 and y(Si) > 0.15 the system becomes Type I. (The top of the valence band is also in the Ge layer).

[0065]   Our synthetic strategy for preparation of Ge-Sn-Si structures is focused on reactions of the gaseous compound SiH_3-GeH_3 with SnD_4. The former is a simple derivative of GeH_3-GeH_3 in which one of the GeH_3 groups is replaced with the SiH_3 analog thus forming a molecular core with direct Si-Ge bonds. A result of these reactions is presented by the RBS spectruma in Fig. 11. The spectrum is obtained from a sample with concentration $Si_{0.13}Ge_{0.82}Sn_{0.05}$ grown on Si(100) via a $Ge_{0.95}Sn_{0.05}$ buffer layer at 350°C. Ion beam channeling indicates single phase, epitaxial and highly crystalline material. Ongoing experiments have resulted in growth of $Ge_{1-x-y}Si_xSn_y$ with a wider range of compositions. It is noteworthy that growth of SiGeSn on pure Si surfaces (no Ge-Sn buffer layers) yields SiGeSn quantum dots and large scale islands of composition $(SiGe)_{1-x}Sn_x$ rather than layers These results are described below in the discussion of nanostructures.

[0066]   We have investigated the optical properties of SnGeSi alloys. In particular, the results we have already obtained for Sn_xGe_{1-x} alloys suggest that linear interpolations may not be justified in this system, so that device applications of SnGeSi alloys will require a detailed characterization of its electronic structure. We are conducting systematic studies of the electronic structure of these novel alloys using spectroscopic ellipsometry and photoreflectance.

High efficiency IR detectors based on Ge-Sn/Ge heterostructures

As discussed above, high-quantum efficiency sensing devices can be designed based on simple $Sn_{1-x}Ge_x$/Ge heterostructures grown on Si. In collaboration with Dr. Richard Soref at the Air Force Labs, one embodiment of such a device for 1.55 μm detection has been proposed, as shown in FIG. 12. A preferred arrangement for such a device involves a Ge(0.98)Sn(0.02)-buffered single "optically thick" active layer of compressively strained Ge(0.96)Sn(0.04) upon which a tensile cladding of Ge is grown. This is one embodiment of a group of single-layer or "few layer" sensors for 1.55 μm that are easy to manufacture using our method.

Synthesis of ordered phases with composition $Ge_{4-5}Sn$

[0067]   We have conducted investigations of structure vs. composition in the Ge-Sn system to search for novel ordered phases that are likely to have unique and exciting properties, such as high electron mobilities and direct band gaps. We have discovered that the compositional range $Sn_{0.17-0.20}Ge_{0.83-0.80}$ displays an unusual ordering of the atoms in the structure, as shown in FIG. 13. Thin epitaxial films of these materials were grown on Si(100) and Si(111) substrates and characterized by RBS, x-diffraction and high-resolution electron microscopy, including extensive Z-contrast and electron energy loss spectroscopy (EELS) analyses at 1.7 Å resolution. The structural investigations indicate the existence of a superstructure that has a periodicity along the <111> direction that is three times larger than that of the underlying substrate. *Ab initio* density functional theory simulations were used to elucidate the structural and bonding behavior of this material. The experimental and theoretical data point to novel phases in which the Ge and Sn atoms are aligned in the sequences of Ge-Ge-$Sn_{0.50}Ge_{0.50}$ and Ge-$Sn_{0.25}Ge_{0.75}$-$Sn_{0.25}Ge_{0.75}$ along the diamond <111> direction. The theoretical studies provide structural models that are consistent with the composition as well as the spectroscopic, microscopic and diffraction data of this material. FIG. 14 depicts models of the layered Ge_5Sn alloys consistent with the Z-contrast atomic resolution microscopy. Orthorhombic cells derived from the zincblende lattice. The long axis of the orthorhombic cells is topotactic with the [111] direction in the original zincblende lattice. Individual layers are denoted by L_1, L_2 and L_3. The left model, denoted by "0-0-50" represents the extreme, tin-rich scenario in which half of the sites within one layer are occupied by tin, while the right model, "0-25-25" the tin concentration is distributed among two layers.

GeSn, Ge, and SiGeSn Nanostructures Grown on Silicon

[0068]   In accordance with another aspect of the invention, we have developed a new family of semiconductor quantum dots (QDs) with tunable direct bandgaps in the infrared spectral region for Si-based bandgap and lattice engineering applications. This effort is a rational outcome of the successful synthesis of epitaxial layers of $Ge_{1-x}Sn_x$ (x=0.02-0.20) alloys with adjustable direct band gaps between 0.72 eV and 0.41 eV described above. Closely related nanoscale architectures with unusual morphologies and nearly perfect crystallinities have been created via new methods combing specially designed molecular sources and novel deposition

techniques involving *in situ* observation and control of the growth process by LEEM and UHV-SEM-MBE. An important component of the work is the design and selection of precursors that incorporate the necessary building blocks to allow precise control of composition and structure at the nanoscale.

Synthesis of $Ge_{1-x}Sn_x$ quantum dots

[0069] The successful synthesis of Sn-Ge epitaxial films on Si prompted us to undertake the growth of related nanostructures such as alloy quantum dots and three-dimensional islands to further explore tailoring the optical properties of this novel system. Ge-Sn nanostructues with direct tunable bandgaps combined with the underlying Si substrate (which is indispensable for viable device development) should have tremendous potential for use in infrared laser technologies.

[0070] A survey of preliminary experiments of quantum dot growth was conducted in a molecular beam epitaxy chamber equipped with a low energy electron microscope (LEEM), allowing the entire growth process to be observed and controlled *in situ* and in real time. The precursor gases (Ge_2H_6 and SnD_4) were adjusted in the reaction mixture so as to incorporate Sn concentration of about 2-3 at. % in the alloy. FIG. 15 shows a sequence of LEEM images from an 8-μm diameter area of GeSn growth at 400°C. The terraces, which are separated by single-height atomic steps, alternate from dark to bright contrast due to the rotation of the dimer reconstruction on the terraces, as shown in the first image in FIG. 15. As the GeSn film was deposited on the Si(100) substrate, the contrast of each terrace was changing from dark to bright or from bright to dark respectively. The contrast alternation indicates that the growth mode is layer-by-layer. The LEEM results reveal that at least for the first six monolayers, the $Ge_{1-x}Sn_x$ deposition takes place by the layer-by-layer growth mode. However, the contrast faded away permanently as the coverage exceeded 6 ML indicating transition to a three dimensional island like growth mechanism. Continued deposition generated the desired assemblies of $Ge_{1-x}Sn_x$ quantum dots. The average Ge and Sn concentration was determined by RBS to be $Ge_{0.97}Sn_{0.03}$. Atomic force microscopy (AFM) indicated the presence of three-dimensional faceted islands dispersed on the surface of the substrate. XTEM revealed that the material consisted of a continuous and completely epitaxial wetting layer, about 0.4 nm thick, followed by an array of nanoscale bump-shaped islands randomly distributed on the surface of the

16

underlying layer. The presence of the wetting layer is consistent with the LEEM observations of two-dimensional layer-by-layer growth for the first six monolayers.

[0071]   A XTEM micrograph showing representative islands grown on Si(100) is presented in FIG. 16. The smaller island shown in FIG. 16A is highly strained and completely coherent and defect free despite the large mismatch of the Ge-Sn material with the substrate. The larger island of FIG. 16B shows defects such as misfit dislocations and {111} stacking faults indicating that this material has exceeded a critical thickness beyond which the enormous strain is relieved by development of defects originating at the film/substrate interface.   The combination of nanostructures and the technologically relevant Ge-Sn system is unique and warrants further development. Of immediate interest is to measure the optical properties by IR absorption and photoreflectance. Once the bandgap energy is determined, we will investigate the luminescence of the quantum dots. A detailed investigation of the crystal growth fundamentals is also of interest.   One of the objectives is to achieve regular in-plane distribution of semiconductor quantum dots that have sufficient size uniformity and spatial distribution. Such arrays are desirable for their potentially useful optical and electronic properties.   Another objective is to determine the optical properties as a function of Sn concentration. An immediate goal is to grow quantum dots with concentration of $Ge_{0.86}Sn_{0.14}$, which has been shown to exhibit a very small direct bandgap in bulk films. In addition the synthesis of new materials with wider concentration range is being pursued.

Quantum dots with highly controlled concentrations in the Si-Ge-Sn system

[0072]   The successful formation of $Ge_{1-x}Sn_x$ quantum structures is prompting exploratory research aimed at synthesis of ternary Si-Ge-Sn alloy analogs. A reason for interest in alloys in the Si-Ge-Sn system is the observation that the lattice parameter of Ge (5.66 Å) is intermediate between those of Si (5.43 Å) and α-Sn (6.49 Å). Thus a Ge-Si material containing a suitable level of Sn would lattice match Ge, thereby allowing growth of strain free heteroepitaxial layers films on Ge buffer layers. Moreover, this ternary system offers the potential of bandgap engineering and tuning of the optical properties, as indicated by theoretical studies.   Our initial deposition studies of Si-Ge-Sn were conducted by UHV-CVD reactions using H_3GeSiH_3 (a unimolecular precursor with direct Si-Ge bonds) as the source of Si and Ge.

17

H_3SiGeH_3 is a stable and gaseous compound and it is synthesized by using a new and high yield method outlined by the equation

$$C_4F_9SO_3SiH_3 + KGeH_3 \rightarrow H_3SiGeH_3 + KO_3SC_4F_9$$
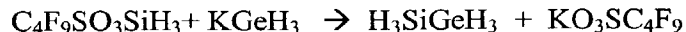
[0073] Prior to growing Si-Ge-Sn on Si(100) via this method we performed controlled experiments involving the thermal dehydrogenation of H_3SiGeH_3 to study the deposition characteristics of the compound on Si(100) between 350 °C and 700 °C. XTEM and AFM were used to characterize the structure and morphology of the films. The microscopy data revealed that all depositions invariably produced assemblies of highly coherent quantum dots on the Si surface instead of smooth and continuous films. The shape, distribution and size of the dots were closely dependent on the temperature pressure and growth rate of the sample.

[0074] FIGs. 17A, 17B and 17C show XTEM images of monocrystalline defect free dots grown under a wide range of conditions. Spatially resolved electron energy loss spectroscopy was used (EELS) was used to examine the elemental content of the dots. An extensive survey of samples revealed that the distributions of the constituent elements were homogeneous at every nanoscale region probed and that the concentration of all islands was extremely close to the stochiometric SiGe value regardless of growth conditions. The incorporation of the entire Si-Ge molecular core of H_3SiGeH_3 in nanoscale islands indicates that reactions of the compound with suitable Sn sources such as SnD_4 is likely to yield $(SiGe)_{1-x}Sn_x$ dots with highly controlled concentrations at the atomic level. Initial growth experiments using this method produced films with average composition ranging from $(SiGe)_{0.90}Sn_{0.10}$ to $(SiGe)_{0.85}Sn_{0.15}$, indicating that the elemental ratio can be adjusted by building the desired stoichiometries into a unimolecular precursor. XTEM and SEM studies revealed an array of crystalline nano-size islands on the Si surface (FIGs. 18A-D) instead of continuous layers. The Raman shifts and the lattice constants of this material indicate Sn incorporation into SiGe tetrahedral sites and high-resolution XTEM images demonstrated nearly perfect heteroepitaxial growth, as shown in FIGs. 18A-18D. Nanoprobe EDX elemental profiles show that Si, Sn and Ge were present at each nanometer step probed. The analyses revealed no significant variations in composition within an island, and only minor discrepancies in Sn content between islands.

[0075]   The incorporation of Sn in SiGe islands provides yet another alloy system to practice bandgap engineering in IR semiconductor nanostructures. Immediate investigations are focused on generating uniform distributions of coherent islands with uniform size and spatial distribution. An objective is to determine optical and electronic properties as a function of composition and size. Future studies will concentrate on the influence of the Sn content on the morphology, structure and optical properties of $(SiGe)_{1-x}Sn_x$ nanostructures. Another important issue to be resolved is the origin of the unusual crystal growth observed in this system. Similar nanoscale features have not yet been observed in systems comprising group IV elements such as Ge, $Si_{1-x}Ge_x$ and $Ge_{1-x}Sn_x$. The morphological evolution of island formation in the $(SiGe)_{1-x}Sn_x$ system will be studied *in situ*, in real time using the LEEM method and a UHV SEM-MBE built by Delong Instruments of the Czech Republic for Arizona State University in Tempe, Arizona which is intended to be used for *in situ* studies of three-dimensional growth.

(Ge Si₄)₁₋ₓSnₓ quantum dots and related systems

[0076]   The incorporation of the entire Si-Ge molecular core of the H_3SiGeH_3 compound in $(SiGe)_{1-x}Sn_x$ nanoscale islands indicates that compositional control can be achievable at the atomic level in ternary semiconductor nanostructures via deposition of related compounds with chemically designed stoichiometries and atomic arrangements. The compounds will have the general formula $A(BH_3)_4$ where {A,B}={Si,Ge,Sn}. FIG. 19 shows a schematic representation of the $A(BH_3)_4$ cluster. These compounds are designed to introduce into the film building blocks such the $SnGe_4$ and $SnSi_4$ $GeSi_4$ and $GeSi_4$ tetrahedral clusters, thus allowing manipulation of the composition and structure at the atomic level. We note that in some cases isolated Sn atoms are bonded within a Ge or Si environment thus promoting the highest possible Sn substitution into the structure. In addition the use of such precursors will allow us to overcome thermodynamic impediments arising from differences in atomic sizes and electronegativities of constituent atoms and thereby form new and metastable compositions, which cannot be obtained by conventional MBE and CVD routes. Using this approach, we will be able to controllably deposit new families of semiconductor nanostructures of definite composition in the Si-Ge-Sn system.

[0077]   Initial growth studies are underway to synthesize Si-Ge-Sn alloy dots by reactions of SnD_4 with $Ge(SiH_3)_4$, a stable and volatile compound (vapor pressure 15 Torr at

22°C) incorporating the desired GeSi$_4$ building units. Prior to these studies, we conducted controlled deposition involving thermally activated dehydrogenations of the Ge(SiH$_3$)$_4$ between 450°C and 650°C in order to determine the unimolecular decomposition behavior of this species. Thin films were grown and characterized for structure and morphology by XTEM and AFM. The data revealed that the depositions produced periodic arrays of large three-dimensional islands instead of the anticipated continuous layer morphology. High-resolution XTEM electron micrographs (FIGs. 20A-B) show completely epitaxial and nearly defect-free microstructure with fairly uniform size, shape and spatial distribution. The elemental concentration of individual islands was determined by spattialy resolved EELS to be Si$_{0.80}$Ge$_{0.20}$, which matches exactly the 4:1 atomic ratio of Si and Ge in the precursor. This result indicates that the entire Si$_4$Ge core stoichiometry and possibly tetrahedral structure of the precursor is incorporated into the solid state. We will conduct growth of quantum dots by reactions of the compound with SnD$_4$. These reactions are likely to yield dots with target stoichiometries of (Si$_4$Ge)$_{1-x}$Sn$_x$ incorporating highly uniform concentrations at the atomic level. A highly suitable precursor to Ge-Sn and Si-Ge-Sn nanostructures is the Sn(GeH$_3$)$_4$ compound, which consists of a central Sn atom surrounded by Ge atoms. It is highly likely that the unimolecular deposition of the precursor will produce single-phase alloy nanostructures with concentration Ge$_{0.80}$Sn$_{0.20}$ that incorporate the entire Ge$_4$Sn molecular stoichiometry. This Ge$_{0.08}$Sn$_{0.20}$ composition is desirable because it is within the range of Ge-Sn compositions that yield direct bandgaps.

Wires and islands of Ge$_{1-x}$C$_x$ alloys on a nanometer scale

[0078]   A major reason for interest in alloys of the Ge-C system is the observation that the lattice parameter of Si (5.43Å) is intermediate between those of Ge (5.66Å) and diamond (3.57Å). Thus a Ge material containing a suitable level of C would exactly match the lattice parameter of Si, allowing growth of strain-free heteroepitaxial layers. This simple binary alloy system offers the potential of bandgap engineering. However, in contrast to the well-known SiC, stoichiometric GeC has never been synthesized. The preparation of Ge$_{1-x}$C$_x$ alloys, especially those with high C content, thus presents a serious challenge.

[0079]   We have recently discovered that reactions utilizing unimolecular precursors of CH$_x$(GeH$_3$)$_{4-x}$ where x = 0-3, result in the formation of Ge-C materials which display unusual morphologies and microstructure depending on the molecular design of the

20

precursor and the C concentration. For example, reactions of CH_3GeH_3 with GeH_4 on Si(001) substrates resulted in low growth rates but high-quality epitaxial films of $Ge_{1-x}C_x$ with C = 2-5 at. %. Decomposition reactions of the precursor $C(GeH_3)_4$ at $530^{\circ}C$ under CVD conditions produced $Ge_{1-x}C_x$ films with C content close to 9% grown on Si(001) substrates. FIG. 21 is an XTEM image of a $Ge_{0.91}C_{0.09}$ island grown on the surface of Ge-C epitaxial layer. The Ge-C layer has a thickness of about 20 nm and the Ge-C island has a size of ~70 nm. An ensemble of such nano-scale islands is shown in the AFM image in the inset of FIG. 21.

[0080] Our most recent deposition experiments using the precursor $CH_2(GeH_3)_2$ produce a dense array of nanowires or nanorods as shown in the SEM images in FIGs. 22A and 22B. These filament-like wires or rods grew from a 40 nm $Ge_{1-x}C_x$ epitaxial film with x = 13%. The orientations of the Ge-C filaments are random, as shown in FIGs. 22A and 22B. It is our objective to fabricate well-oriented filaments or nano-pillars.

[0081] All the above results are highly reproducible, suggesting the possibility of growing novel Ge-C nanostructures, which may be beneficial in the design and fabrication of electronic devices. The optical properties of these materials are of tremendous interest and are presently being more thoroughly investigated. The possibility exists of discovering direct bandgap materials in the Ge-C system. Potential field emission from the nano-pillars will be also investigated.

CONCLUSION

[0082] The above-described invention possesses numerous advantages as described herein and in the referenced appendices. The invention in its broader aspects is not limited to the specific details, representative devices, and illustrative examples shown and described. Accordingly, departures may be made from such details without departing from the spirit or scope of the general inventive concept.

References
1. E. H. Parker and T. E. Whall, Solid State Electronics **43**, 1497 (1999).
2. M. Quillec, in *Critical Issues in Semiconductor Materials and Processing Technologies* (Kluwer Academic Publishers, Dordrecht, Netherlands, NATO Advanced Study Institute on Semiconductor Materials and Pocessing Technologies, 1992).
3. O. Madelung, *Semiconductors--basic data* (Springer, Berlin, New York, 1996).
4. M. L. Cohen and J. R. Chelikowsky, *Electronic Structure and Optical Properties of Semiconductors* (Springer, Heidelberg, Berlin, New York, 1989).

5.   D. W. Jenkins and J. D. Dow, Phys. Rev. B **36**, 7994 (1987).
6.   K. A. Mader, A. Baldereschi, and H. von Kanel, Solid State Commun. **69**, 1123 (1989).
7.   R. F. C. Farrow, et al., J. Cryst. Growth **54**, 507 (1981).
8.   H. Höchst, M. A. Engelhardt, and D. W. Niles, SPIE Procedings **1106**, 165 (1989).
9.   C. A. Hoffman, *et al.*, Phys. Rev. B **40**, 11693 (1989).
10.   W. Wegscheider, K. Eberl, U. Menczigar, and G. Abstreiter, Appl. Phys. Lett. **57**, 875 (1990).
11.   O. Gurdal, *et al.*, Appl. Phys. Lett. **67**, 956 (1995).
12.   P. R. Pukite, A. Harwit, and S. S. Iycr, Appl. Phys. Lett. **54**, 2142 (1989).
13.   G. He and H. A. Atwater, Phys. Rcv. Lctt. **79**, 1937 (1997).
14.   L. Bellaiche, S.-H. Wei, and Z. Zunger, Phys. Rev. B **54**, 17568 (1996).
15.   J. Taraci, J. Tolle, M. R. M. Cartney, J. Mcncndcz, M. A. Santana, D. J. Smith, and J. Kouvetakis, App. Phys. Lett. **78**, 3607 (2001).
16.   M. Bauer, J. Taraci, J. Tolle, A. V. G. Chizmeshya, S.Zollner, D. J. Smith, J. Menendez, C. Hu, and J. Kouvetakis, Ge-Sn Semiconductors for Band-gap and Lattice Engineering, App. Phys. Lett. **81**, 2992 (2002).
17.   J. Taraci, S. Zollner, M. R. McCartney, J. Menéndez, M. A. Santana, D. J. Smith, A. Haaland, A. V. Tutukin, G. Gundersen, G. Wolf, and J. Kouvetakis, J. of the Am.Chem. Soc., (2001).
18.   Matthew Bauer, A.V.G. Chizmeshya. D.J. Smith, Jose Menendez, and J. Kouvetakis, *to be published in Solid State Communication.* (2003).
19.   R. A. Soref and L. Friedman, Superlattices and Microstructures **14**, 189 (1993).
20.   K. W. Böer, *Survey of Semiconductor Physics: electrons and other particles in bulk semiconductors* (Van Nostrand Reinhold, Ncw York, 1990).
21.   R. A. Soref and C. H. Perry, J.Appl. Phys. **69**, 539 (1991).
22.   Matthew Bauer, Cole Ritter, P. Crozier, Jie Ren, Josc Menendez, and J. Kouvetakis, *submitted to Applied Physics Letters* (2003).

WHAT IS CLAIMED IS:

1.   A semiconductor structure comprising: a substrate and a Sn_xGe_{1-x} layer formed over the substrate, wherein x has a value from about 0.02 to about 0.30.

2.   The semiconductor structure of claim 1 wherein the Sn_xGe_{1-x} layer is an epitaxial layer with a direct band gap between about 0.72eV and about .041eV.

3.   The semiconductor structure of claim 1, wherein x has a value near 0.20 and the Sn_xGe_{1-x} layer is a direct-gap material.

4.   The semiconductor structure of claim 1, wherein the substrate comprises a silicon substrate.

5.   The semiconductor structure of claim 3 wherein the substrate comprises Si(100).

6.   The semiconductor structure of claim 3 wherein the substrate comprises Si(111).

7.   The semiconductor structure of claim 1, wherein the substrate comprises a silicon substrate and the $Sn_{1-x}Ge_x$ layer is formed directly on the substrate.

8.   The semiconductor structure of claim 7 wherein the substrate comprises Si(100).

9.   The semiconductor structure of claim 7 wherein the substrate comprises Si(111).

10.   The semiconductor structure of claim 1 wherein the Sn_xGe_{1-x} layer has a thickness from about 50nm to about 500nm.

11.   The semiconductor structure of claim 1 further comprising a strained Ge layer formed over the Sn_xGe_{1-x} layer.

12.   The semiconductor structure of claim 11 wherein x is greater than about 0.11 and the strained Ge layer is a direct-gap material.

13.   The semiconductor structure of claim 1 wherein the Sn_xGe_{1-x} layer is doped with an element selected from the group consisting of P, As and Sb.

23

14.   The semiconductor structure of claim 1 further comprising a Ge-Sn-Si layer formed over the Sn_xGe_{1-x} layer.

15.   A semiconductor structure comprising: a Ge-Sn quantum structure formed over a silicon substrate.

16.   The semiconductor structure of claim 15 wherein the Ge-Sn quantum structure comprises $Ge_{1-x}Sn_x$ and x has a value from about 0.02 to about 0.03.

17.   The semiconductor structure of claim 15 wherein the Ge-Sn quantum structure is formed over Ge-Sn epitaxial layer formed over the silicon substrate.

18.   The semiconductor structure of claim 15 wherein the substrate comprises Si(100).

19.   A semiconductor structure comprising a Si-Ge-Sn quantum structure formed over a silicon substrate.

20.   The semiconductor structure of claim 19 wherein the Si-Ge-Sn quantum structure comprises $(SiGe)_{1-x}Sn_x$ and x has a value from about 0.02 to about 0.15.

21.   The semiconductor structure of claim 19 wherein the Si-Ge-Sn quantum structure comprises $(Si_4Ge)_{1-x}Sn_x$ and x has a value from about 0.00 to about 0.99.

22.   The semiconductor structure comprising: a silicon substrate and a $Ge_{1-x}C_x$ epitaxial layer formed over the substrate, wherein x has a value from about 0.02 to about 0.13.

23.   The semiconductor structure of claim 22 further comprising a Ge-C quantum structure formed over the epitaxial layer.

24.   The semiconductor structure of claim 22 further comprising Ge-C nanowires formed over the subtrate.

25.   A method for depositing an epitaxial Ge-Sn layer on a substrate in a chemical vapor deposition reaction chamber, the method comprising introducing into the chamber a

gaseous precursor comprising SnD_4 under conditions whereby the epitaxial Ge-Sn layer is formed on the substrate.

26. The method of claim 25 wherein the gaseous precursor comprises SnD_4 and high purity H_2.

27. The method of claim 25 wherein the gaseous precursor comprises high purity H_2 of about 15-20% by volume.

28. The method of claim 25 wherein the gaseous precursor is introduced at a temperature in a range of about 250°C to about 350°C.

29. The method of claim 25 wherein the substrate comprises silicon.

30. The method of claim 29 wherein the silicon comprises Si(100).

31. The method of claim 25 wherein the Ge-Sn layer comprises Sn_xGe_{1-x} and x is in a range from about .02 to about .20.

32. A method for depositing a strained Ge layer on a silicon substrate with a Ge-Sn buffer layer in a chemical vapor deposition reaction chamber, the method comprising introducing into the chamber a combination comprising SnD_4 and Ge_2H_6 under conditions whereby the Ge-Sn layer is formed on the substrate and dehydrogenating Ge_2H_6 under conditions whereby the Ge layer is formed on the Ge-Sn buffer layer.

33. A method for doping a region of a semiconductor material in a chemical vapor deposition reaction chamber, the method comprising introducing into the chamber a gaseous precursor having the formula $E(GeH_3)_3$, wherein E is selected from the group consisting of arsenic, antimony and phosphorus.

34. The method of claim 33 wherein the semiconductor material comprises silicon.

35. The method of claim 33 wherein the semiconductor material comprises

germanium.

36. The method of claim 33 wherein the semiconductor material comprises SiGeSn.

37. The method of claim 33 wherein the semiconductor material comprises SnGe.

38. A method for synthesizing a compound having the formula $E(GeH_3)_3$ wherein E is selected from the group consisting of arsenic, antimony and phosphorus, the method comprising combining GeH_3Br with $[(CH_3)_3Si]_3E$ under conditions whereby $E(GeH_3)_3$ is formed.

39. A method for synthesizing a compound having the molecular formula $H_3Si-GeH_3$, the method comprising combining $H_3SiO_3SCF_3$ with $KGeH_3$ under conditions whereby H_3SiGeH_3 is formed.

40. A method for incorporating Sn into Ge or GeSi, the method comprising comprising mixing H_2 with SnD_4 to stabilize the SnD_4 and using the stabilized SnD_4 as a source of Sn atoms.
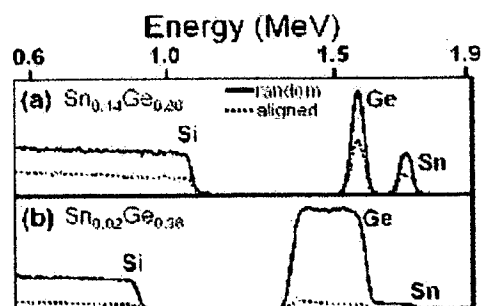
FIG. 1A   FIG 1B
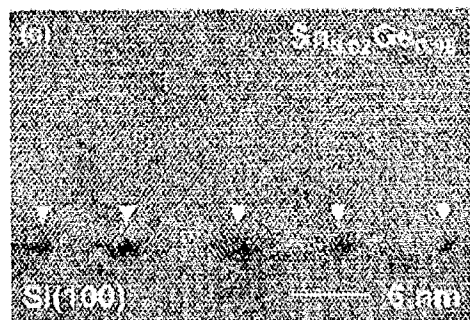
FIG. 1C
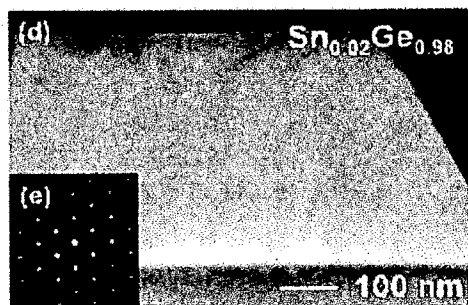
FIG. 1D   FIG. 1E
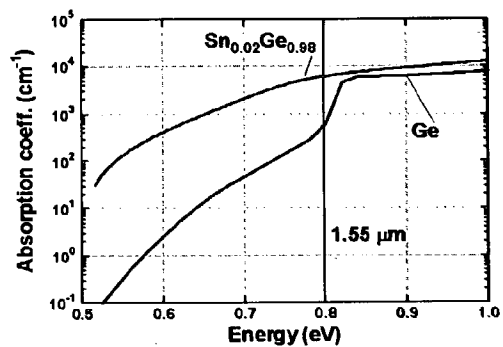
FIG. 2
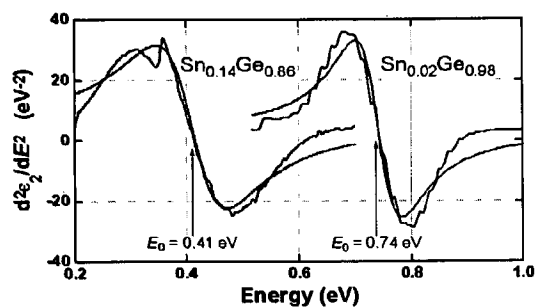
FIG. 3
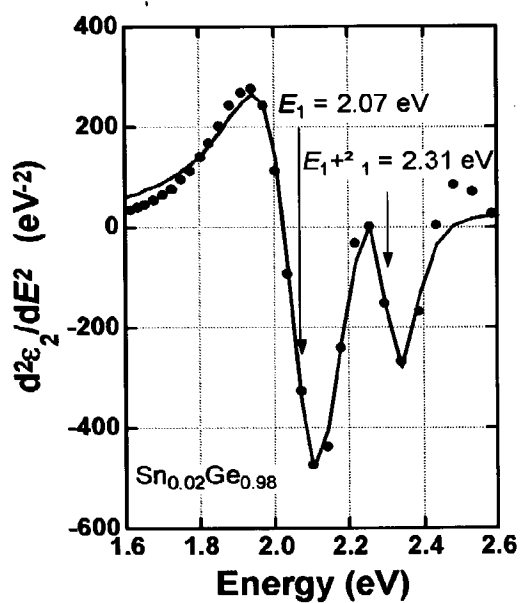
FIG. 4
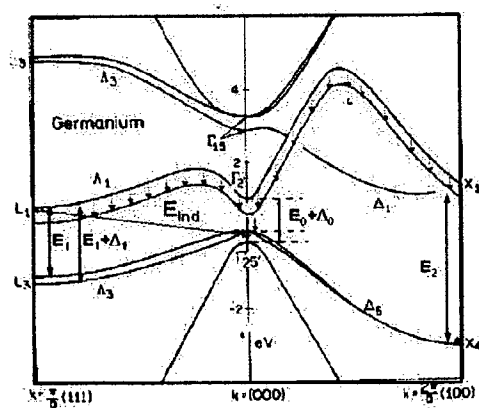
FIG. 5
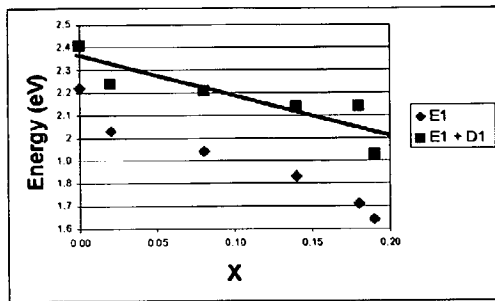
FIG. 6A
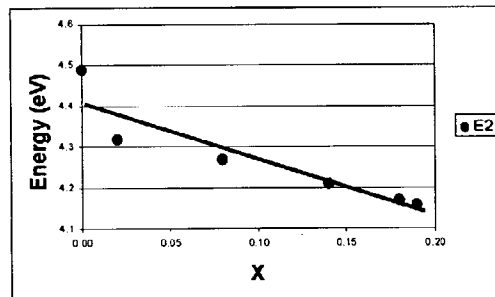
FIG. 6B
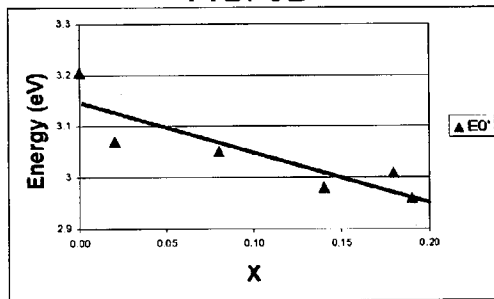
FIG. 6C
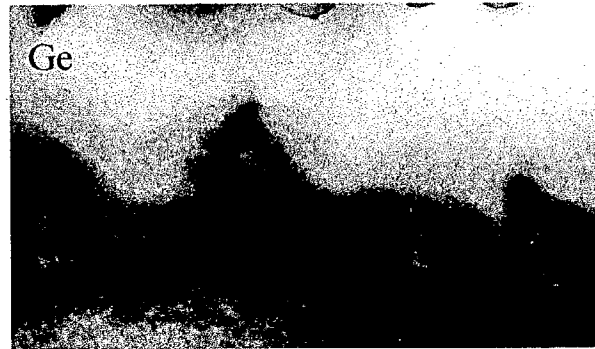
FIG. 8
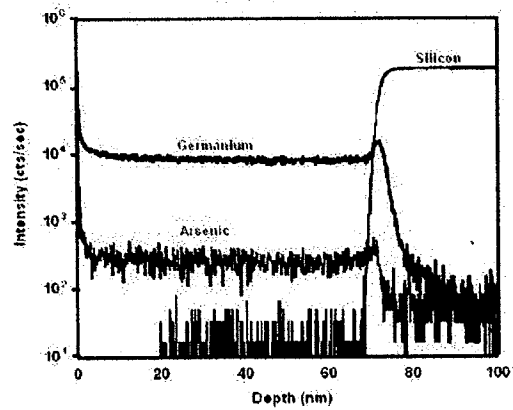
FIG. 9
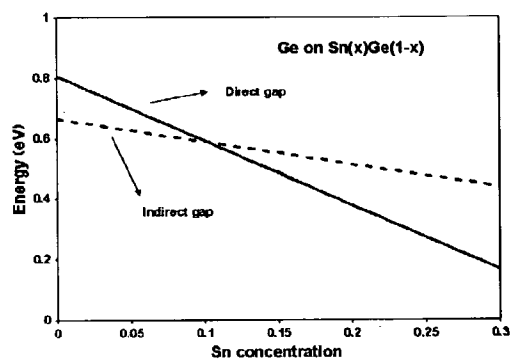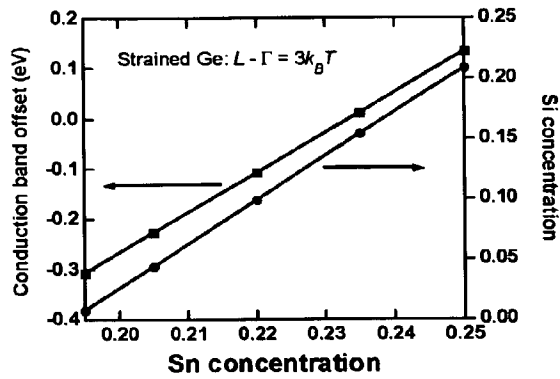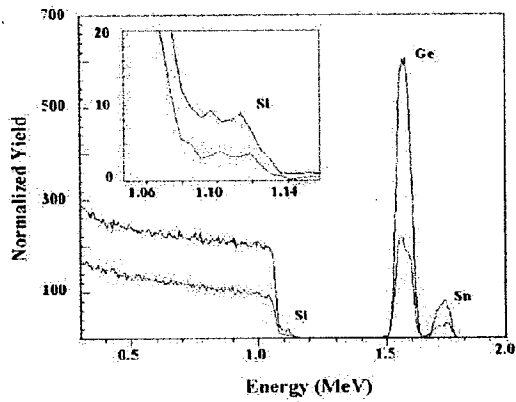

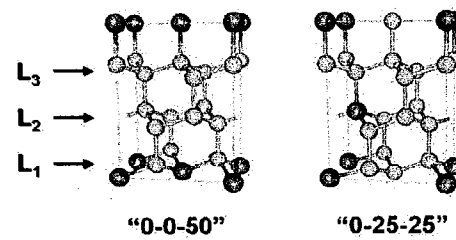FIG. 7

FIG. 10

FIG. 11

FIG. 13

"0-0-50"   "0-25-25"

FIG. 14

FIG. 12

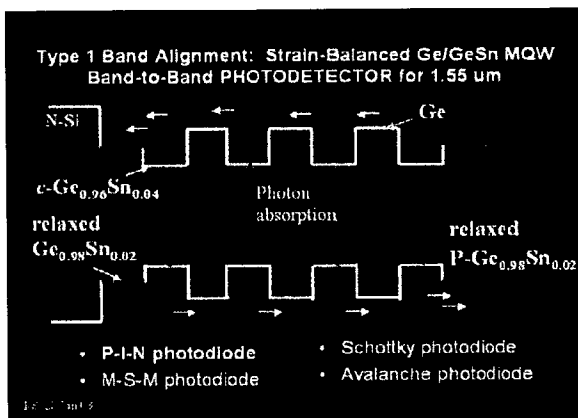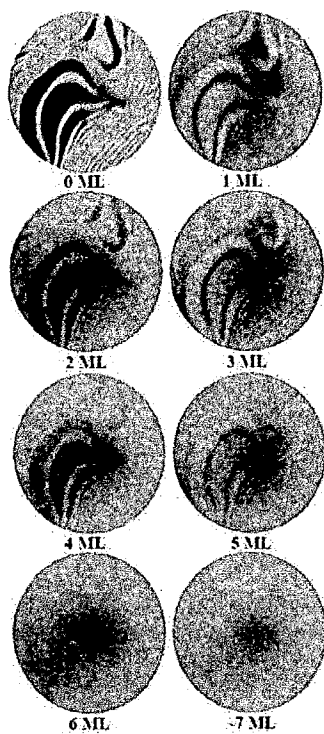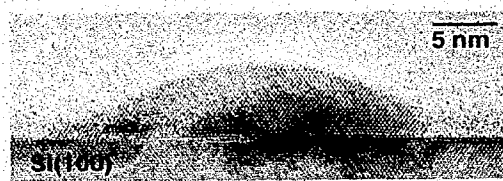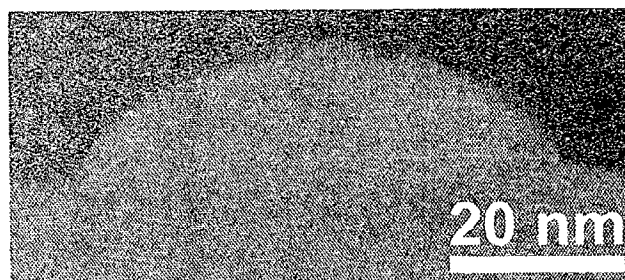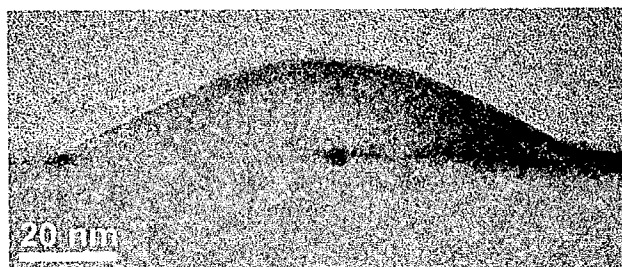3 / 5

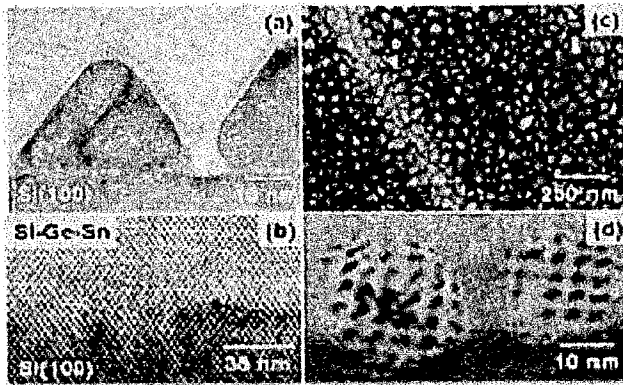FIG. 15

FIG. 16A

FIG. 16B
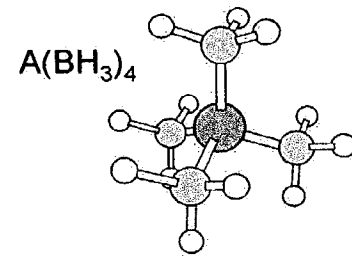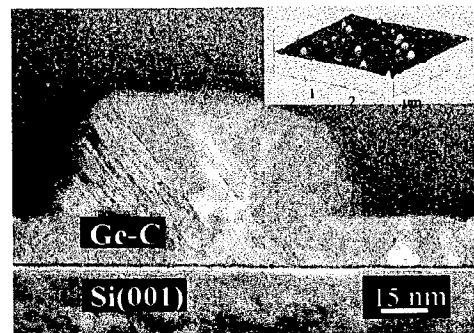

FIG. 17B

FIG. 17C

FIG. 17A

4 / 5

FIG. 18

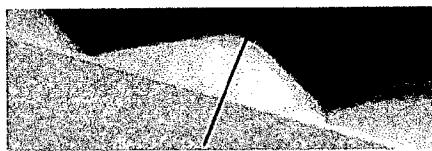$A(BH_3)_4$
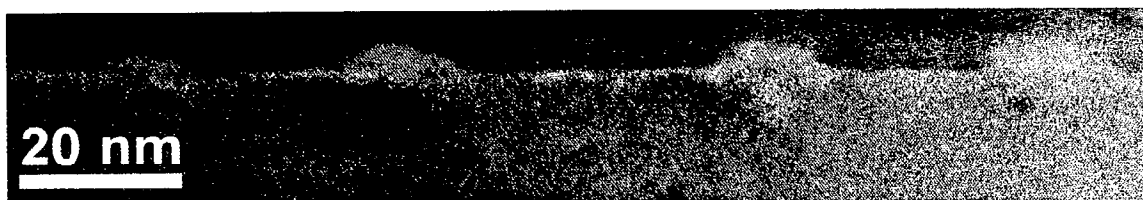
FIG. 19

FIG. 21
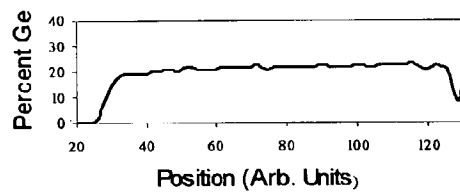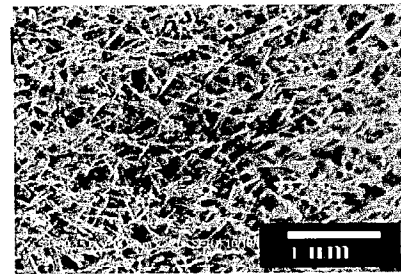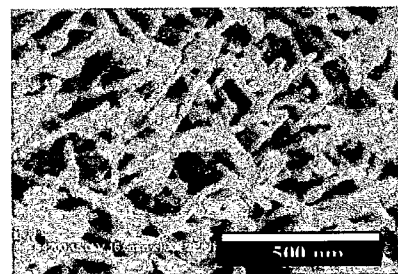

FIG. 20A

FIG. 20B

FIG. 20C

FIG. 22A

FIG. 22B

5 / 5

Ge–Sn semiconductors for band-gap and lattice engineering

M. Bauer,[a] J. Taraci,[a] J. Tolle,[a] A. V. G. Chizmeshya,[b] S. Zollner,[c]
David J. Smith,[b],[d] J. Menendez,[c] Changwu Hu,[d] and J. Kouvetakis[a]
*Arizona State University, Tempe, Arizona 85287 and Motorola Inc, 2200 West Broadway, Mesa,
Arizona 85202*

We describe a class of Si-based semiconductors in the $Ge_{1-x}Sn_x$ system. Deuterium-stabilized Sn hydrides provide a low-temperature route to a broad range of highly metastable compositions and structures. Perfectly epitaxial diamond-cubic $Ge_{1-x}Sn_x$ alloys are grown directly on Si(100) and exhibit high thermal stability, superior crystallinity, and crystallographic and optical properties, such as adjustable band gaps and lattice constants. These properties are completely characterized by Rutherford backscattering, low-energy secondary ion mass spectrometry, high-resolution transmission electron microscopy, x-ray diffraction (rocking curves), as well as infrared and Raman spectroscopies and spectroscopic ellipsometry. *Ab initio* density functional theory simulations are also used to elucidate the structural and spectroscopic behavior. © *2002 American Institute of Physics.* [DOI: 10.1063/1.1515133]

Development of $Ge_{1-x}Sn_x$ alloys with diamond-cubic structures has attracted considerable attention because of predictions that Ge–Sn heterostructures might exhibit tunable direct bandgaps.[1,2] From a synthesis viewpoint, the major problem with Sn incorporation into the Ge lattice is the large (17%) lattice mismatch between the elements and the instability of the diamond-cubic structure of α-Sn above 13 °C.[3] Accordingly, the thermodynamic solubility of Sn in Ge is less than 0.5 at. %, while that of Ge in Sn is zero.[4] $Ge_{1-x}Sn_x$ alloys are thus unstable and their synthesis requires conditions that are far from equilibrium. Nevertheless, significant efforts have been devoted to growing $Ge_{1-x}Sn_x$ alloys by molecular beam epitaxy (MBE) using nonequilibrium conditions.[1,3,5] A major problem encountered with MBE is the propensity of Sn to segregate toward the film surface.[3,6] To counteract this effect, MBE growth of Ge–Sn must be conducted at very low temperatures, that is, ~ 100 °C, placing a severe limit on the film critical thickness. Under these conditions Ge–Sn alloys have been reported to grow as thin and highly strained layers.[3] However, only strain-free materials are predicted to exhibit direct band gaps.

Our work in this area has focused on development of chemical methods to synthesize device quality $Ge_{1-x}Sn_x$ structures on Si with a wide range of single-phase compositions that may not be accessible by conventional MBE.[7] In this letter we describe systematic growth and characterization of *unstrained* $Ge_{1-x}Sn_x$ alloys with concentrations of 2–17 at. % Sn prepared directly on Si(100) substrates. The observed crystal properties are superior to those of pure Ge films grown on Si, indicating that Sn incorporation in tetrahedral Ge sites, even at modest concentrations, leads to structural and strain behavior compared to Ge, Si–Ge, and related systems. The key to the synthesis is the development of a low temperature pathway based on reactions of stabi-

lized gaseous SnD_4, the simplest possible and highly practical Sn source.

Depositions were conducted in a UHV-chemical vapor deposition reactor at substrate temperatures between 250 and 350 °C at 10^{-3} Torr. The Si(100) wafers were prepared for growth by a modified RCA process followed by hydrogen surface passivation. The reaction of SnD_4 with Ge_2H_6 on Si produced epitaxial $Ge_{1-x}Sn_x$ films. Rutherford backscattering (RBS) revealed that thick layers (50–500 nm) with Sn contents of 13 to 17 at. % were deposited reproducibly between 290 and 250 °C, respectively. Depositions at higher temperatures between 300 and 350 °C gave Sn contents of 12 to 2 at. %, respectively, indicating an inverse dependence of the growth temperature on Sn incorporation. To determine the quality of epitaxial growth and evaluate the Sn substitutionality, RBS random and aligned spectra were recorded. Figure 1 shows the spectra for samples containing 2% and 12% Sn. Both Sn and Ge channel remarkably well despite the large difference in lattice constant with the substrate. The channeling of Sn provides unequivocal proof that this element must occupy substitutional tetrahedral sites. The extent of substitutionality can be assessed by comparing the values of χ_{min} between Ge and Sn in the same sample (χ_{min} is the ratio of the aligned versus random peak height). The value of χ_{min} is 4%, for both Ge and Sn in the $Ge_{0.98}Sn_{0.02}$ sample and 35% in the $Ge_{0.88}Sn_{0.12}$ sample indicating that the entire Sn content is substitutional. The 4% value approaches the practical limit of about 3% for structurally perfect Si, which is unusual for a binary crystal grown directly on Si. The 35% value is relatively high and is likely due to some mosaic spread in the higher Sn-content crystal due to the increase in lattice mismatch. Low-energy secondary ion mass spectrometry showed background levels of D, H, and C and revealed highly uniform Sn and Ge elemental profiles throughout the film. Homogeneity at the nanometer scale was confirmed using energy dispersive x-ray nanoanalysis in a high-resolution electron microscope with probe size less than 1 nm. Compositional profiles showed homogeneous Ge and Sn distribution

[a]Department of Chemistry and Biochemistry.
[b]Center for Solid State Science.
[c]Motorola Inc, 2200 West Broadway, Mesa AZ 85202
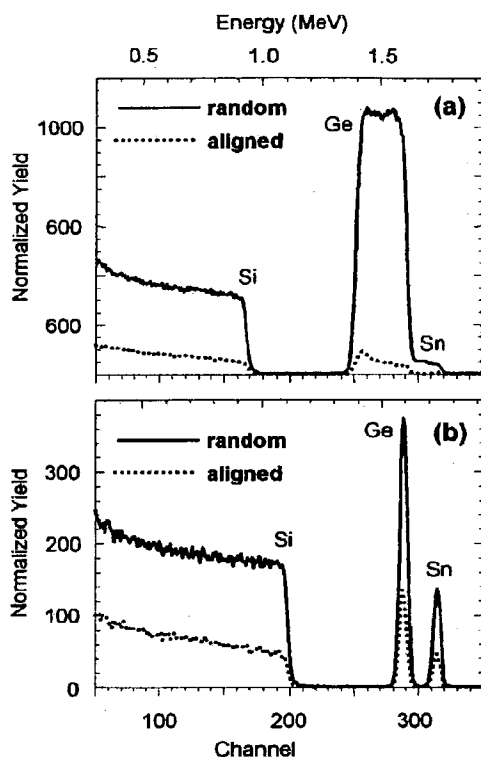[d]Department of Physics and Astronomy.

Appendix A

Appl. Phys. Lett., Vol. 81, No. 16, 14 October 2002

Bauer *et al.* 2993

FIG. 1. (a) RBS aligned (dotted line) and random (solid line) spectra of $Ge_{0.98}Sn_{0.02}$ with near perfect crystallinity. Channeling of Sn and Ge approaches the theoretical limit of pure Si. (b) Aligned and random spectra for $Ge_{0.88}Sn_{0.12}$ show the same χ_{min} for both Ge and Sn indicating that the entire Sn content is substitutional.

FIG. 2. Cross-sectional electron micrographs of $Ge_{0.94}Sn_{0.06}$. Top panel shows atomically flat film surface morphology, middle panel shows the exceptional uniformity of the film thickness. Bottom panel is a high-resolution electron micrograph of the interface region showing virtually perfect epitaxial growth. Arrows indicate the location of misfit dislocations.

with no evidence of phase separation or Sn precipitation.

The structural properties of the films were investigated by cross-sectional electron microscopy (XTEM) and high resolution x-ray diffraction. The XTEM studies revealed thick single-crystal layers with remarkably low concentrations of threading defects. Electron micrographs demonstrating high quality heteroepitaxial growth of $Ge_{0.94}Sn_{0.06}$ are shown in Fig. 2. Typical images in the (110) projection show occasional threading dislocations and {111} stacking faults sometimes extending through to the uppermost surface. The estimated density of these defects is $\sim 10^7/cm^2$, a value well within the levels considered acceptable for device application. The predominant defects accommodating the large misfit are Lomer edge dislocations at the interface which are parallel to the interface plane and should not degrade electrical properties and device performance. Finally, the film surface is virtually flat at the atomic level. The typical rms roughness of 0.5 to 1.4 nm, as observed by atomic force microscopy, is comparable to atomic step heights on Si surfaces.

X-ray measurements in the θ–2θ mode showed a strong peak corresponding to the (004) reflection. In-plane rocking scans of the (004) reflection have a full width at half maximum between 0.25 and 0.50 degrees, indicating a tightly aligned spread of the crystal mosaics. The unit cell parameters obtained from the (004) reflection for samples containing 2, 3, 4, 9, 11, and 15 at.% Sn (as measured by RBS)
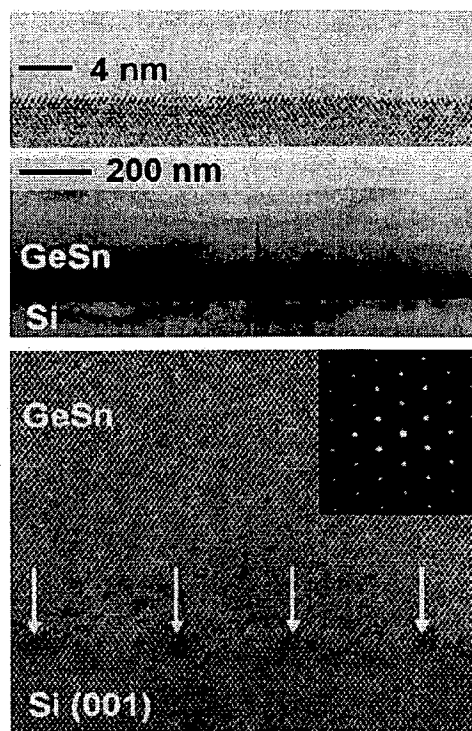
were 5.6720, 5.6936, 5.7111, 5.7396, 5.7611, and 5.802 Å respectively. These values are intermediate to those of Ge (5.658 Å) and α-Sn (6.493 Å), and they increase monotonically with increasing Sn concentration. Virtually identical values were obtained from the selected area electron diffraction patterns. Digital diffractogram analysis of TEM micrographs confirmed the measured values of the unit cell constants and also showed that the lattice parameter did not vary locally throughout the sample.

The Sn concentration as measured by RBS, the corresponding cell parameter estimated from Vegard's law, a(Vegard), and the experimental unit cell parameters a are listed in Table I. Also included are the results of theoretical calculations, based on *ab initio* density functional theory, for the lattice constants as a function of Sn. There is close agreement between theory and experiment. A striking feature is that a positive deviation from Vegard's law is found for both the experimental and theoretical values, which is in direct contrast with the compositional variation of the lattice constant in the classic $Si_{1-x}Ge_x$ and $Si_{1-x}C_x$ group IV alloys. In these systems the deviations from Vegard's law are usually negative.[8,9]

In order to further characterize the local bonding environment in the Ge–Sn lattice, the Raman spectrum of each sample was acquired. The materials showed a strong peak corresponding to Ge–Ge phonon mode, which is downshifted substantially with respect to pure Ge. The vibrational

2994   Appl. Phys. Lett., Vol. 81, No. 16, 14 October 2002

Bauer et al.

TABLE I. Observed and calculated lattice parameters. The observed lattice parameter composition dependence in the range 0%–15% Sn content is compared with Vegard's law. The calculated values are obtained from a first-principles local density approximation static lattice calculation. The "relaxed" results correspond to fully optimized structures.

	Observed			Calculated	
% Sn	a(Vegard)	a(observed)	Sn/Ge	a(Vegard)	a(relaxed)
0	5.658	5.658	0	5.626	5.626
2	5.675	5.672	1/64	5.639	5.639
3	5.683	5.694	2/64	5.652	5.653
4	5.691	5.711	4/64	5.678	5.683
9	5.733	5.740	8/64	5.729	5.737
11	5.750	5.761	12/64	5.781	5.792
15	5.783	5.802	1	6.456	6.456

frequencies decrease monotonically with increasing Sn concentration due to the combined effects of mass substitution and elongation of the average Ge–Ge bond distances. The compositional dependence of the Ge–Ge frequency shift can be fitted with an expression of the form $\Delta\omega(x) = -72x$ (in cm^{-1}) where x is the Sn concentration. This dependence agrees well with an extrapolation of similar results for strain-free $Si_{1-x}Ge_x$ and $Si_{1-x}C_x$ alloys based on a simple model for the compositional dependence of Raman modes in alloy semiconductors.[10]

The Ge–Sn samples were annealed between 400 and 750 °C to determine their thermal stability. The x-ray lattice parameter and the χ_{min} values of the RBS signals were measured and compared with the pre-annealed values, and XTEM and nanoprobe energy dispersive x-ray analysis were used to determine phase separation and any elemental inhomogeneity. Samples with composition $Ge_{0.98}Sn_{0.02}$ were remarkably stable up to at least 750 °C and showed an improvement in crystallinity with increasing temperature. The $Ge_{0.95}Sn_{0.05}$ composition remained robust up to 600 °C, but displayed substantial Sn precipitation between 600–700 °C. In the case of the $Ge_{0.88}Sn_{0.12}$ and $Ge_{0.85}Sn_{0.15}$ compositions, the corresponding thermal stability range was reduced to below ~500 and ~450 °C, respectively.

The band structure of the Ge–Sn materials was investigated by resonant Raman scattering and spectroscopic ellipsometry.[11] The Raman cross section in pure Ge undergoes a resonant enhancement for laser photon energies near the E_1 and $E_1 + \Delta_1$ gaps.[12] We performed similar measurements for a $Ge_{0.95}Sn_{0.05}$ alloy and a Ge reference. The net result was a redshift of E_1 and $E_1 + \Delta_1$ by about 100 meV relative to pure Ge. Ellipsometric data were acquired in the 1 to 6 eV photon-energy range for samples containing between 5% to 15% Sn. The imaginary part ε_1 of the pseudodielectric function shows peaks between 1.5 and 2.5 eV corresponding to E_1 and $E_1 + \Delta_1$, a shoulder at 3.5 eV assigned to the E_0 transition, and a feature at 4.2 eV corresponding to the E_2 gap. These peaks indicate a well-defined band structure as expected for a crystalline film with long-range ordering. We were able to obtain an accurate determination of the E_2 critical point, which showed that the gap values varied monotonically from 4.32 to 4.27 eV compared to 4.37 eV in pure Ge and 3.63 eV in pure Sn. The band gaps obtained from ellipsometry and from the maxima of the Raman excitation profiles are compared in Fig. 3 with a linear interpolation of
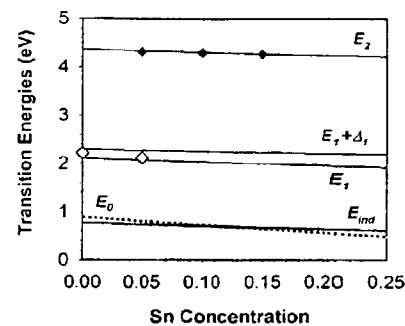

FIG. 3. Resonant Raman scattering and spectroscopic ellipsometry data for the E_1 (hollow symbols) and E_2 (filled symbols) transitions in $Ge_{1-x}Sn_x$, indicating gap narrowing with increasing Sn concentration. The bottom two traces are the fundamental direct (E_0) and indirect (E_{ind}) gaps. The solid lines represent a linear interpolation between the known band structure of pure Ge and pure α-Sn (fundamental direct gap shown as a dashed line).

the E_2, E_1 and $E_1 + \Delta_1$ transition energies between known values for Ge and α-Sn.[13] The figure also shows a linear interpolation for the indirect (E_{ind}) and direct (E_0) edges, demonstrating a transition near $x = 0.15$. This estimate agrees well with more sophisticated calculations of the band structure of these alloys.[2] Collectively, the data indicate that we have synthesized alloys with compositions in the range, which should exhibit a transition from indirect to direct band gap behavior.

To verify this experimentally we have performed IR transmission measurements for several samples in the range of 2000 and 10 500 cm^{-1}. While the exact location of the absorption edges has not yet been determined, our results clearly show that between 4000 and 8000 cm^{-1} the absorption coefficient increases monotonically by a substantial amount with increasing Sn content. The most plausible explanation is a decrease of the band gap as a function of composition, since such a reduction is likely to result in increased absorption at a fixed photon energy above the bandgap.

[1] G. He and H. A. Atwater, Phys. Rev. Lett. 79, 1937 (1997).
[2] D. W. Jenkins and J. D. Dow, Phys. Rev. B 36, 7994 (1987).
[3] O. Gurdal, R. Desjardins, J. R. A. Carlsson, N. Taylor, H. H. Radamson, J.-E. Sundgren, and J. E. Greene, J. Appl. Phys. 83, 162 (1998).
[4] Bull. Alloy Phase Diagrams 5, 266 (1984), and references therein.
[5] M. T. Asom, E. A. Fitzgerald, A. R. Kortan, B. Spear, and L. C. Kimerling, Appl. Phys. Lett. 55, 578 (1989).
[6] W. Wegscheider, J. Olajos, U. Menczigar, U. Dondl, and G. Abstreiter, J. Cryst. Growth 132, 75 (1992).
[7] J. Taraci, J. Tolle, J. Kouvetakis, M. R. McCartney, D. J. Smith, J. Menendez, and M. A. Santana, Appl. Phys. Lett. 78, 3607 (2001).
[8] Z. Charafi and N. Bouarissa, Phys. Lett. A 234, 493 (1997).
[9] H. Kajiyama, S-I. Muramatsu, T. Shimada, and Y. Nishino, Phys. Rev. B 45, 14005 (1992).
[10] J. Menendez, in Raman Scattering in Materials Science, edited by W. H. Weber and R. Merlin (Springer, Berlin, 2000), pp. 55–103.
[11] W. Richter, Resonant Raman Scattering in Semiconductors, in Springer Tracts in Modern Physics, Vol. 78, edited by G. Hohler (Springer, New York, 1976), p. 121.
[12] F. Cerdeira, W. Dreyrodt, and M. Cardona, Solid State Commun. 10, 591 (1972).
[13] L. Vina, H. Hochst, and M. Cardona, Phys. Rev. B 31, 958 (1985).

Tunable Band Structure in Diamond-cubic Tin-Germanium Alloys Grown on Silicon Substrates

Matthew R. Bauer[1], John Tolle[1], Corey Bungay[2], Andrew V.G. Chizmeshya[3], David J. Smith[3,4], José Menéndez[4*], and John Kouvetakis[1]

[1]Department of Chemistry and Biochemistry, Arizona State University, Tempe, Arizona 85287-1604

[2]J. A. Woollam Co., Inc., 645 M Street, Lincoln, Nebraska 68508 USA

[3]Center for Solid State Science, Arizona State University, Tempe, Arizona 85287-1704

[4]Department of Physics and Astronomy, Arizona State University, Tempe, Arizona 85287-1504

Novel chemical methods based on deuterium-stabilized Sn hydrides and ultra-high-vacuum chemical vapor deposition were used to grow Sn_xGe_{1-x} alloys directly on silicon. Device-quality, strain free films with a Sn-fraction as high as $x = 0.2$ were obtained. The optical properties provide evidence for a well-defined Ge-like band structure. In particular, the direct band gap E_0 is reduced to a value as low as 0.41 eV for $Sn_{0.14}Ge_{0.86}$. The growth of these high-optical quality infrared materials creates entirely new opportunities for band gap engineering on Si.

78.20.Ci, 81.15.Kk, 71.55.Cn

*jose.menendez@asu.edu

Appendix B

The physical properties of most semiconductor alloys are smooth functions of their composition, providing a very versatile tool for device engineering. Alloys of elemental semiconductors such as Si and Ge, and alloys of III-V compounds such GaAs, AlAs, InAs, and InP, play a key role in high-speed microelectronics[1] and in optoelectronics.[2] In particular, the group-IV Ge_xSi_{1-x} system is a nearly ideal semiconductor alloy, with a lattice constant and interband optical transition energies that are essentially linear functions of x.[3] An even more intriguing group-IV alloy is the Sn_xGe_{1-x} system. Group-IV semiconductors are notorious for not displaying a direct band gap, which precludes their use as active layers in light-emitting diodes and lasers. The band gap of the Sn_xGe_{1-x} alloy, however, is expected to undergo an indirect-to-direct transition, since the direct band gap has a value of 0.81 eV in Ge and becomes negative (-0.4 eV) in gray (α-) Sn.[4] A linear interpolation between Ge and α-Sn places the crossover at $x = 0.2$, and this simple estimate agrees remarkably well with detailed electronic structure calculations within the virtual crystal approximation.[5][6]

Unfortunately, the growth of Sn_xGe_{1-x} alloys has been hampered by the enormous lattice mismatch (15%) between Ge and α-Sn and the instability of the cubic α-Sn structure above 13°C. As a result the system is highly metastable and cannot be produced in bulk form. However, the reported stabilization of α–Sn in films grown by molecular beam epitaxy (MBE)on InSb and CdTe substrates[7] encouraged several groups to attempt the growth of Sn_xGe_{1-x} using the same procedure. Significant progress has been made,[8][9] but the large compositional dependence of the lattice constant limits this approach to a narrow range of compositions near the Sn-rich end. For the technologically more interesting Ge-rich Sn_xGe_{1-x} alloys, pure Ge is an obvious choice as a substrate, and in

2

fact fully strained Sn_nGe_m superlattices[10] as well as random Sn_xGe_{1-x} alloys[11] on Ge have been demonstrated. Unfortunately, a major disadvantage of Ge substrates is that tetragonally distorted Sn_xGe_{1-x} films on Ge are not expected to display an indirect-to direct transition. Strain-free Ge-rich Sn_xGe_{1-x} films have been grown by Pukite, Harwit, and Iyer[12] and by He and Atwater[13] on Si substrates using Ge buffer layers. The optical properties of these films, however, differ very markedly[13] from those observed in conventional semiconductor alloys: individual interband transitions are not observed, and the position of the band edges is obtained from fits that must incorporate transitions not found in pure Ge.

The unusual optical properties of relaxed Sn_xGe_{1-x} alloys[13] suggest that it may not be possible to describe the Sn_xGe_{1-x} system in terms of an effective band structure, as is usually done with well-behaved semiconductor alloys. An anomalous dependence of the physical properties on composition has in fact been predicted for alloys of very different materials, such as GaAsN,[14] and given the large mismatch between Ge and Sn, similar findings would not be entirely surprising for Sn_xGe_{1-x} alloys. If this were the case, the possible applications of Sn_xGe_{1-x} alloys would be severely limited. In this letter, however, we report on the optical properties of strain-free Sn_xGe_{1-x} films grown directly on Si by a novel CVD method. Unlike previous results, our films show clear evidence for a well-defined Ge-like band structure, demonstrating that Sn_xGe_{1-x} alloys are viable candidates for a variety of novel devices based solely on group-IV materials.

The CVD sources that are normally used in the synthesis of Si-based semiconductors are SiH_4 and GeH_4. The analogous SnH_4 molecule is unstable near room temperature due to the low Sn-H bond energy, and is thus unsuitable for deposition applications. Since the

3

substitution of deuterium for hydrogen should increase the kinetic stability of the molecules, we have recently experimented with (Ph)SnD$_3$ and SnD$_4$ as possible sources for the growth of Sn-based semiconductors.[15] In the case of pure SnD$_4$, the enhanced stability provided by D is insufficient at 22°C, but we discovered that the combination of SnD$_4$ with high-purity H$_2$ (15-20% by volume) remains remarkably stable at 22°C for extended time periods. This formulation represents the simplest possible source of Sn atoms for the growth of novel Sn-Ge systems.

Depositions were conducted in a custom-built ultra-high-vacuum CVD reactor on Si(001) wafers. Growth temperatures between 250 °C and 350 °C produced thick films (50-500 nm) with Sn concentrations up to 19%, as measured by Rutherford backscattering (RBS). Figure 1(a) and 1(b) shows a comparison between random and aligned RBS spectra for a Sn$_{0.02}$Ge$_{0.98}$ sample and a Sn$_{0.14}$Ge$_{0.86}$ sample. The ratio χ_{min} between the aligned and random peak heights measures the degree of channeling of the incoming He ions. Its value is 4% in the $x = 0.02$ sample and about 50% in the $x = 0.14$ sample for *both* Ge and Sn. This provides unequivocal proof that Sn occupies substitutional sites in the average diamond structure. To the best of our knowledge, no such quantitative proof of perfect substitutionality has ever been presented for Sn$_x$Ge$_{1-x}$ alloys. The $\chi_{min} = 4\%$ value closely approaches the practical limit of about 3% for structurally perfect Si, which is unprecedented for a binary crystal grown directly on Si. The structural properties of the films were further investigated by high-resolution cross-sectional electron microscopy (XTEM). Electron micrographs demonstrating nearly defect-free growth of Sn$_{0.02}$Ge$_{0.98}$ are shown in Fig. 1(c), 1(d), and 1(e). The images show that the predominant defects accommodating the large misfit between the alloys and the Si substrate are Lomer edge

4

dislocations at the interface (Fig 1c). These are parallel to the interface plane and do not degrade the film quality. A typical image of the entire film thickness in (110) projection (Fig. 1d) shows the presence of occasional threading dislocations and {111} stacking faults, sometimes extending through the uppermost surface. The density of these defects is on the order of $10^7/cm^2$, a value well within the levels considered acceptable for device applications. The surfaces are very smooth, continuous, and atomically flat. The typical root-mean-square surface roughness measured by atomic force microscopy is between 0.5 nm and 1.4 nm, which is comparable to atomic step heights on Si surfaces. Electron and X-ray diffraction experiments show a monotonically increasing average lattice constant as a function of the Sn-concentration, with no evidence for a significant tetragonal distortion. The unit cell parameter obtained from the diffraction data for samples containing 2, 3, 5, 8, 11, 15, 18, and 19 at. % Sn (as measured by RBS) were 5.672 Å, 5.694 Å, 5.711 Å, 5.748 Å, 5.761 Å, 5.802 Å, 5.831 Å, and 5.833 Å, respectively.

The optical properties of our films were investigated with spectroscopic ellipsometry, which yields the complex pseudo-dielectric function $\langle \varepsilon_1 + i\varepsilon_2 \rangle$ and the film thickness. Ellipsometric measurements are particularly challenging in Sn_xGe_{1-x} alloys due to the expected existence of optical transitions from the mid-infrared to the ultraviolet. We used a combination of two instruments. A VASE® (variable angle spectroscopic ellipsometer, J.A. Woollam and Co.) covered the 0.5 eV - 4.1 eV range. This instrument is equipped with a Xenon lamp, a double monochromator, and an extended infrared InGaAs detector.

5

An IR-VASE® (J.A. Woollam and Co.) ellipsometer was used to cover the 0.03 eV - 0.83 eV range. This ellipsometer is based on a Fourier-transform spectrometer. The optical constants for our films were obtained by modeling our samples as three-layer systems comprising a surface layer, the Sn_xGe_{1-x} film, and the Si substrate. Numerical derivatives of the dielectric function were computed and compared with analytical models of the dielectric function near critical points in the electronic joint-density of states.

We focus here on the critical points associated with the E_0 transition and $E_1/E_1+\Delta_1$ transitions, which are schematically indicated in Fig. 2. We show results for two samples: a $Sn_{0.02}Ge_{0.98}$ film and a $Sn_{0.14}Ge_{0.86}$ film. Their thicknesses were found to be 407 nm and 63 nm, respectively. Figure 3 shows the lowest-energy sharp features in the numerical second derivative of ε_2 for the two samples. We assign these features to the E_0 transition, which corresponds to the material's direct band gap. Its value in Ge is 0.81 eV, is slightly above the energy of the lowest indirect gap at 0.66 eV.[16] The critical point associated with E_0 is a three-dimensional minimum M_0, so that the data in Fig. 3 are modeled with an expression of the form $\varepsilon = A\left(E - E_0 + i\Gamma\right)^{1/2} e^{i\phi}$ plus a quadratic background.[17] The amplitude A, the transition energy E_0, and the broadening Γ are taken as adjustable parameters. For a pure three-dimensional minimum, the phase angle ϕ equals $\pi/2$. Here we take ϕ as a fourth adjustable parameter. This allows us to model possible excitonic effects as an admixture of M_0 and M_1 critical points, following a well-established procedure.[17] The fits are performed simultaneously to the real (not shown) and imaginary

6

parts of $d^2\varepsilon/dE^2$. Our results for ε_2 are shown as dashed lines in Fig. 3. We obtain $E_0 =$ 0.740 ± 0.001 eV and $\Gamma = 0.056$ eV for $x = 0.02$ and $E_0 = 0.409 \pm 0.001$ eV and $\Gamma = 0.086$ eV for $x = 0.14$. The phase angle is in both cases near 2.4, revealing strong excitonic effects. In fact, an even better fit of the data can be obtained with a simple Lorenz oscillator model. The E_0 energies obtained from such a fit are virtually unchanged: 0.754 eV for $x = 0.02$ and 0.444 eV for $x = 0.14$. The absorption coefficients at the fitted E_0 values are 3680 cm^{-1} for $x = 0.02$ and 2560 cm^{-1} for $x = 0.14$. These are comparable to the values of the absorption coefficient of pure Ge at its direct band edge,[18] confirming the correctness of our assignments.

Figure 4 shows numerical second derivatives of the dielectric function at energies around 2 eV. For the $x = 0.02$ sample the structures observed are assigned to the E_1 and $E_1+\Delta_1$ transitions. The line shape of the curve is remarkably similar to ellipsometric measurements on pure Ge,[19] providing a dramatic confirmation that the optical properties of our alloys can be understood in terms of a Ge-like band structure. As in the case of pure germanium,[18] the critical points associated with the E_1 and $E_1+\Delta_1$ transitions are modeled as a combination of a two-dimensional minimum with a two-dimensional saddle point: $\varepsilon = C - A \ln (E_t-E-i\Gamma) e^{i\phi}$. For the $x = 0.02$ sample our fit expression includes two such terms, one with $E_t = E_1$ and one with $E_t = E_1 +\Delta_1$. We obtain $E_1 = 2.066 \pm 0.003$ eV with $\Gamma_{E1} = 0.135$ eV, and $E_1 +\Delta_1 = 2.310 \pm 0.003$ eV with $\Gamma_{E1+\Delta1} = 0.082$ eV. The E_1 transition is considerably broadened for the $x = 0.14$ sample, and the $E_1 /E_1+\Delta_1$ doublet cannot be resolved. Hence we include a single critical point, which we continue to refer

7

to as the E_1 transition, although it may contain a mixed $E_1/E_1 + \Delta_1$ character due to alloy mixing. We obtain $E_1 = 1.777 \pm 0.007$ eV with $\Gamma_{E1} = 0.351$ eV.

While the optical data confirm the validity of the effective band structure concept for our Sn_xGe_{1-x} alloys, the large mismatch between Ge and Sn manifests itself in a highly non-linear compositional dependence of the optical properties. This is shown in Figure 5, where the observed energies of the measured interband transitions are compared with theoretical predictions within the virtual crystal approximation. For the E_0 transition we observe a large deviation from a linear interpolation between Ge and α–Sn. This is in sharp contrast with similar measurements in Ge_xSi_{1-x} alloys,[20] for which the E_0 transition energy is a linear function of x. Similarly, the spin orbit splitting Δ_1 shows a large deviation from linearity: if its compositional dependence is fit with a quadratic polynomial of the form $\Delta_1(x) = (1-x)\Delta_1(Ge) + x\Delta_1(Sn) + bx(1-x)$, the resulting "bowing" parameter is $b = 2.2$ eV, almost fifteen times larger than the equivalent bowing parameter in Ge_xSi_{1-x} alloys.[21] The rapid decrease of the E_0 value as a function of the Sn concentration raises the intriguing question as to whether Sn_xGe_{1-x} alloys might become direct gap semiconductors at concentrations much smaller than $x = 0.2$. Unfortunately, the relative lineup of the indirect and direct gaps in our samples cannot be easily extracted from the ellipsometric data, which are rather insensitive to indirect transitions. Photoluminescence measurements would not be conclusive due to the possible proximity of the two transitions and the mutual borrowing of intensity associated with alloy mixing. The most sensitive proof of a direct to indirect cross-over would probably be a

8

measurement of the effective mass of carriers in *n*-type alloys, but these experiments will have to await the development of suitable doping techniques.

In conclusion, we have demonstrated sharp band structure features in the optical properties of Sn_xGe_{1-x} alloys grown directly on Si with a novel CVD method. These alloys should be highly valuable for applications that rely on extending the optical response of Ge towards the infrared.[22] Moreover, since our films grow essentially strain-free, there is in principle no upper limit to the Sn concentration that can be achieved. Thus our approach may represent the most practical solution to the long-standing problem of growing direct-gap semiconductors on Si. In addition, the very large lattice mismatch between our films and the Si substrate opens up intriguing new opportunities for band gap and strain engineering on silicon.

REFERENCES

[1] E. H. Parker and T. E. Whall, Solid State Electronics **43**, 1497 (1999).

[2] M. Quillec, in *Critical Issues in Semiconductor Materials and Processing Technologies* (Kluwer Academic Publishers, Dordrecht, Netherlands, NATO Advanced Study Institute on Semiconductor Materials and Pocessing Technologies, 1992).

[3] O. Madelung, *Semiconductors--basic data* (Springer, Berlin, New York, 1996).

9

[4] M. L. Cohen and J. R. Chelikowsky, *Electronic Structure and Optical Properties of Semiconductors* (Springer, Heidelberg, Berlin, New York, 1989).

[5] D. W. Jenkins and J. D. Dow, Phys. Rev. B **36**, 7994 (1987).

[6] K. A. Mader, A. Baldereschi, and H. von Kanel, Solid State Commun. **69**, 1123 (1989).

[7] R. F. C. Farrow, et al., J. Cryst. Growth **54**, 507 (1981).

[8] H. Höchst, M. A. Engelhardt, and D. W. Niles, SPIE Procedings **1106**, 165 (1989).

[9] C. A. Hoffman, *et al.*, Phys. Rev. B **40**, 11693 (1989).

[10] W. Wegscheider, K. Eberl, U. Menczigar, and G. Abstreiter, Appl. Phys. Lett. **57**, 875 (1990).

[11] O. Gurdal, *et al.*, Appl. Phys. Lett. **67**, 956 (1995).

[12] P. R. Pukite, A. Harwit, and S. S. Iyer, Appl. Phys. Lett. **54**, 2142 (1989).

[13] G. He and H. A. Atwater, Phys. Rev. Lett. **79**, 1937 (1997).

[14] L. Bellaiche, S.-H. Wei, and Z. Zunger, Phys. Rev. B **54**, 17568 (1996).

[15] M. Bauer, *et al.*, Appl. Phys. Lett. **81**, 2992 (2002).

[16] P. Y. Yu and M. Cardona, *Fundamentals of Semiconductors: Physics and Materials Properties* (Springer-Verlag, Berlin, 1996).

[17] D. E. Aspnes, in *Handbook of Semiconductors*, edited by T. S. Moos and M. Balkanski (North Holland, Amsterdam, 1980), Vol. 2.

[18] W. C. Dash and R. Newman, Phys. Rev. **99**, 1151 (1955).

[19] L. Viña, S. Logothetidis, and M. Cardona, Phys. Rev. B **30**, 1979 (1984).

[20] J. S. Kline, F. H. Pollak, and M. Cardona, Helvetica Physica Acta **41**, 968 (1968).

[21] J. H. Bahng, K. J. Kim, S. H. Ihm, J. Y. Kim, and H. L. Park, J. Phys: Condens. Matter **13**, 777 (2001).

[22] R. A. Soref and L. Friedman, Superlattices and Microstructures **14**, 189 (1993).

FIGURE CAPTIONS

Figure 1   Structural characterization of Sn_xGe_{1-x} films on Si. (a) RBS aligned

(dotted trace) and random spectra of $Sn_{0.14}Ge_{0.86}$ showing the same χ_{min} for both Ge

and Sn, indicating that the entire Sn content is substitutional; (b) RBS aligned

(dotted trace) and random spectra of $Sn_{0.02}Ge_{0.98}$ with near perfect crystallinity.

Channeling of Sn and Ge approaches the values found in pure Si; (c) high-resolution

electron micrograph of the film/substrate interface region showing virtually perfect

epitaxial growth. Arrows indicate the location of misfit dislocations; (d) cross section

electron micrograph of $Ge_{0.02}Sn_{0.98}$ showing atomically flat film surface morphology;

(e) Selected-area electron diffraction pattern from $Sn_{0.02}Ge_{0.98}/Si(001)$ interface

region confirming high quality epitaxial growth.

Figure 2   Schematic illustration of a Ge-like band structure in the vicinity of the

fundamental gap. The diagram shows the optical transitions measured by

ellipsometry and the indirect band gap.

Figure 3   Numerical second derivative of the imaginary part of the dielectric

function near the E_0 transition for two Sn_xGe_{1-x} films. The dashed lines shows

theoretical fits, as discussed in the main text.

12

Figure 4 Numerical second derivative of the imaginary part of the dielectric function near the $E_1/E_1+\Delta_1$ transitions for two Sn_xGe_{1-x} films. The dashed lines show theoretical fits, as discussed in the main text.

Figure 5 Compositional dependence of direct and indirect optical transitions in Sn_xGe_{1-x} alloys. The solid lines are linear interpolations between the experimental one-electron band energies in pure Ge and α-Sn. The dashed lines correspond to a tight-binding calculation from Ref. 5. The dashed-dotted lines were computed using a non-relativistic pseudopotential method (Ref. 6). A linear correction has been applied to Refs. 5 and 6 to match the experimentally known room-temperature values in Ge and α-Sn. (a) Lowest direct gap E_0 and indirect band gap E_{ind}. Solid squares are experimental values for the direct gap. The value for $x = 0$ corresponds to pure Ge and has been taken from the literature (Ref. 3); (b) E_1 transition. Circles are experimental values. The value for $x = 0$ corresponds to pure Ge and has been taken from the literature (Ref. 19).

13

Energy (MeV)

(a) $Sn_{0.14}Ge_{0.86}$ —random ......aligned Ge Si Sn

(b) $Sn_{0.02}Ge_{0.98}$ Ge Si Sn
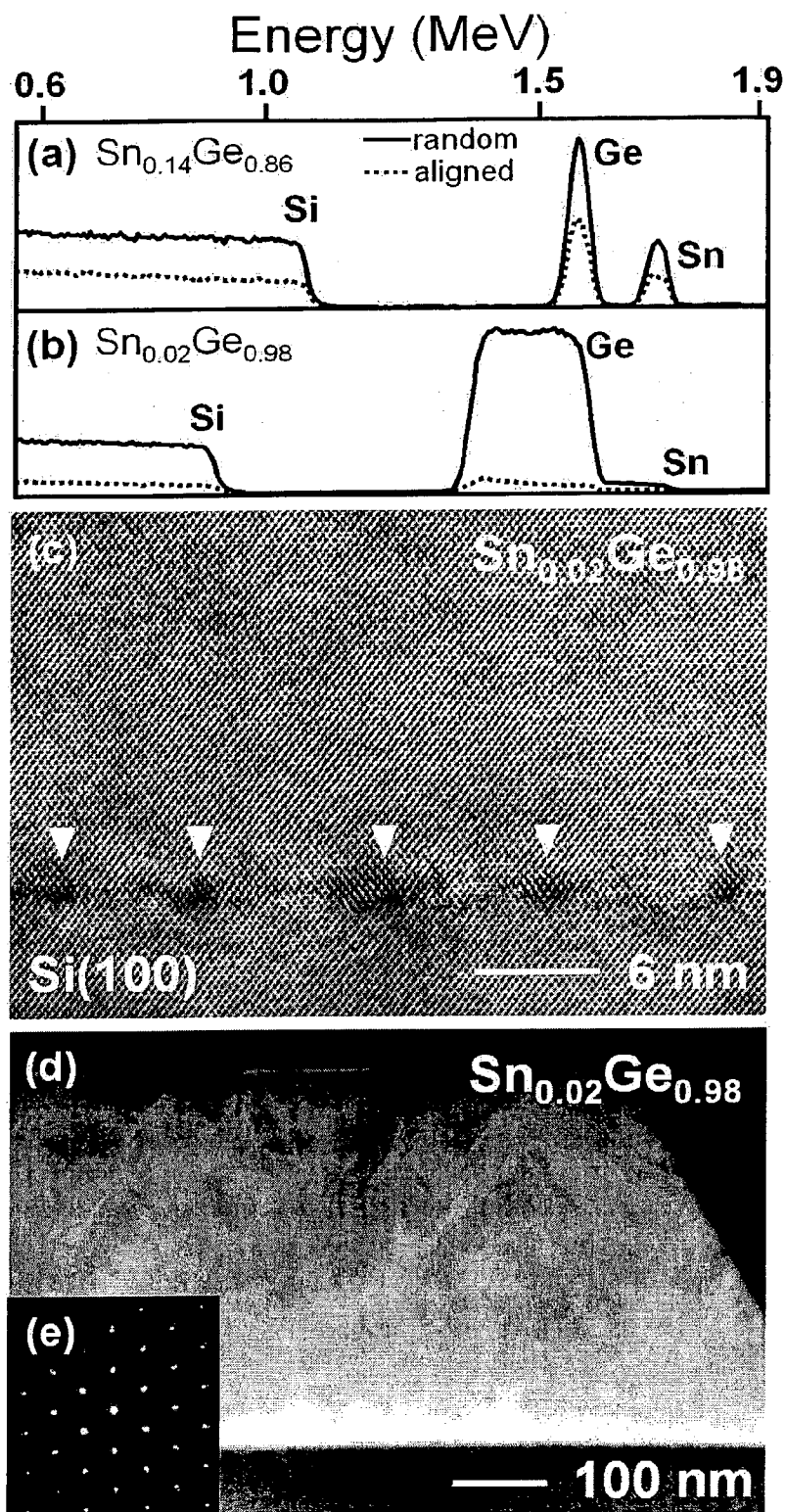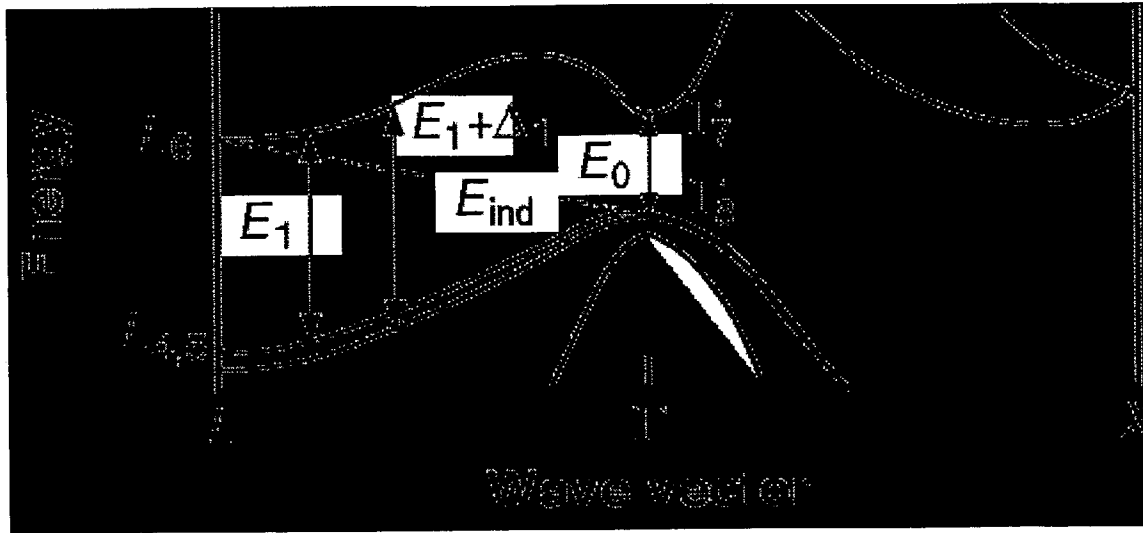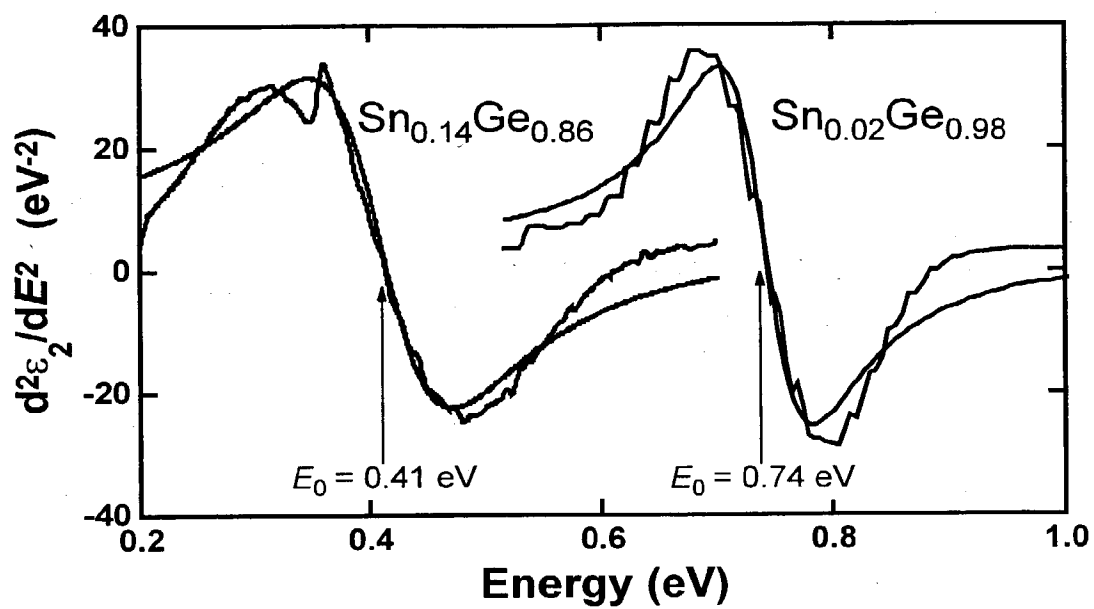
(c) $Sn_{0.02}Ge_{0.98}$ Si(100) 6 nm

(d) $Sn_{0.02}Ge_{0.98}$ (e) 100 nm

Figure 1

Figure 2

Figure 3
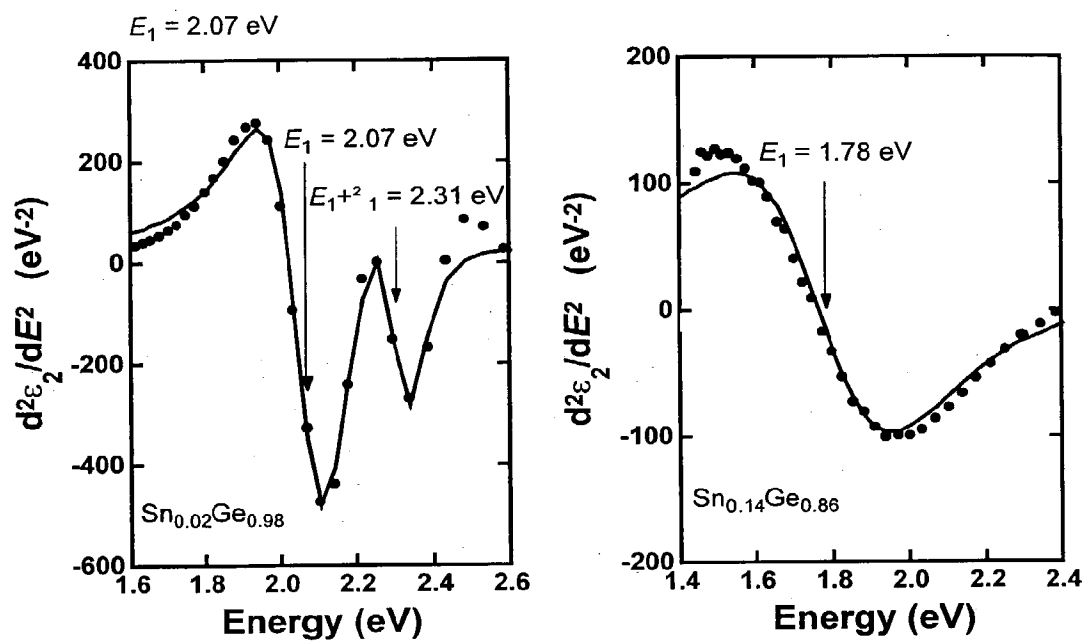
Figure 3

17
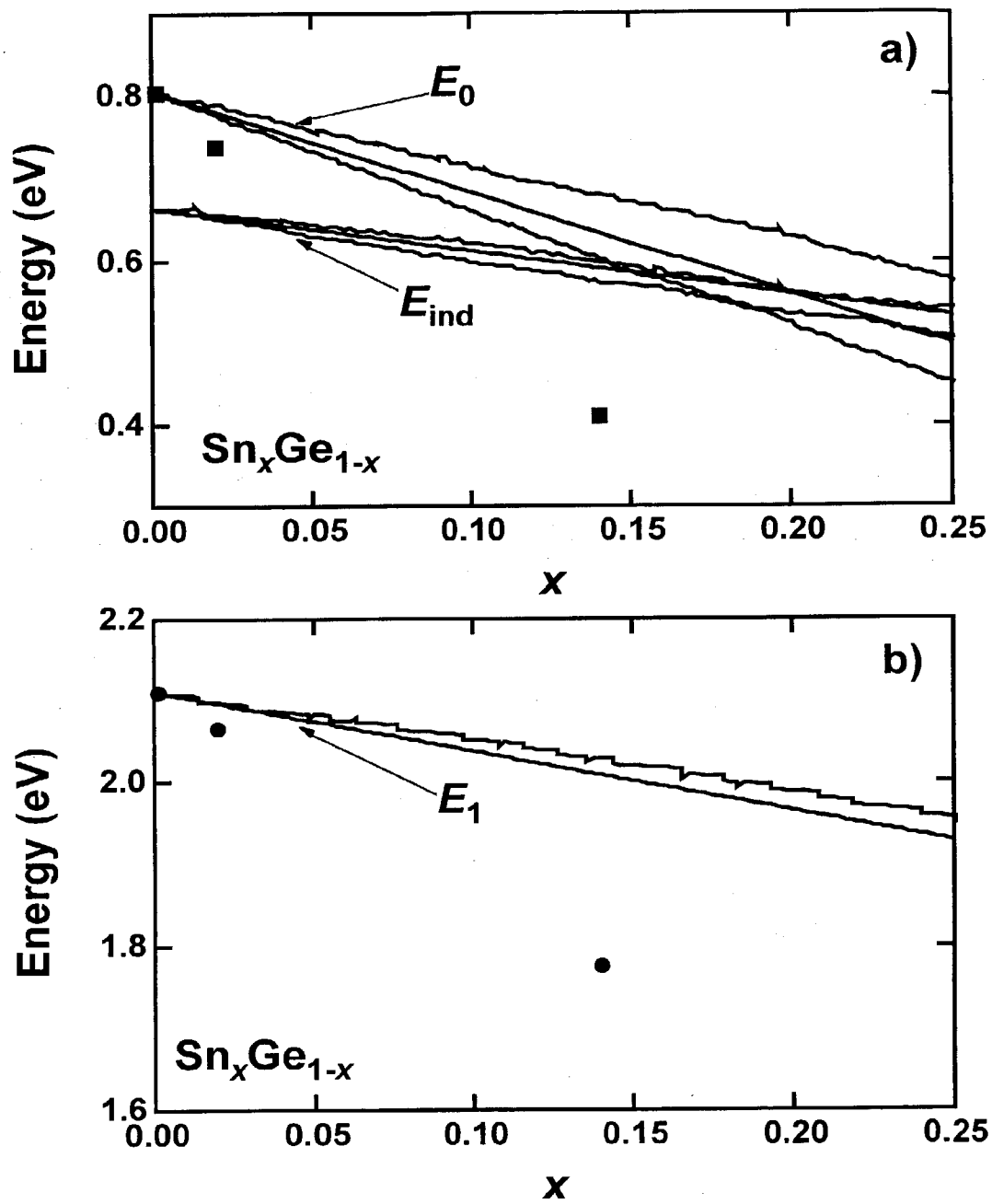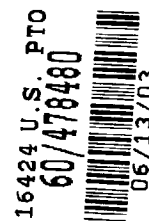
Figure 5

18

Synthesis of Ternary SiGeSn Semiconductors on Si(100) via Sn_xGe_{1-x} Buffer Layers

Matthew Bauer [a], Cole Ritter [a], P. A. Crozier [b], Jie Ren [c], J. Menendez [c], G. Wolf [a]

and J. Kouvetakis [a]

Arizona State University, Tempe, AZ 85287

Abstract

Single-phase $Si_{1-x-y}Ge_xSn_y$ alloys with random diamond cubic structures are created on Si (100) via ultrahigh vacuum chemical vapor deposition reactions of SnD_4 with SiH_3GeH_3 at 350 °C. Commensurate heteroepitaxy is facilitated by $Ge_{1-x}Sn_x$ buffer layers, which act as templates that can conform structurally and readily absorb the differential strain imposed by the more rigid Si and Si-Ge-Sn materials. The crystal structure, elemental distribution and morphological properties of the $Si_{1-x-y}Ge_xSn_y/Ge_{1-x}Sn_x$ heterostructures are characterized by high-resolution electron microscopy, including electron energy loss nanospectroscopy, x-ray diffraction (rocking curves) and atomic force microscopy. These techniques demonstrate growth of perfectly epitaxial, uniform and highly aligned layers with atomically smooth surfaces and monocrystalline structures that have lattice constants close to that of Ge. Rutherford backscattering ion channeling shows that the constituent elements occupy random substitutional sites in the same average diamond cubic lattice and the Raman shifts are consistent with the lattice expansion produced by the Sn incorporation into SiGe tetrahedral sites.

[a] Department of Chemistry and Biochemistry

[b] Center for Solid Sate Science

[c] Department of Physics and Astronomy

Appendix C

1

Introduction

Metastable $Ge_{1-x}Sn_x$ alloys analogous to the well-known $Si_{1-x}Ge_x$ system have attracted considerable attention because of predictions that these materials might possess technologically important electronic properties such as superior electron mobilities and tunable band gaps in the mid infrared.[1,2] More importantly, the band gap is expected to undergo an indirect-to-direct transition at compositions near x = 0.20. Accordingly, considerable efforts have been devoted to growing Ge-rich $Ge_{1-x}Sn_x$ alloys on Ge substrates and buffer layers via MBE methods.[3-5] Recently, we demonstrated, for the first time, the growth of strain-free, device-quality $Ge_{1-x}Sn_x$ films directly on Si substrates using a specially developed ultrahigh vacuum chemical vapor deposition (UHV-CVD) method.[6] The growth proceeds at extremely low temperatures, between 250°C and 350°C, which makes it possible to grow thick films (50-500 nm) with extremely low defect densities and Sn concentrations up to 20%. The films are of such high quality that individual optical transitions can be readily identified and compared with those of pure Ge.[7] In particular, we find a dramatic reduction of the direct band gap E_0, which shrinks from 0.805 eV in pure Ge to 0.41 eV in $Sn_{0.14}Ge_{0.86}$ indicating that these materials might be suitable candidates for a variety of infrared devices, including highly efficiency photodetectors and sensors.

The successful formation of $Ge_{1-x}Sn_x$ films has prompted us to undertake exploratory research aimed at synthesis of the virtually unexplored Si-Ge-Sn ternary analog. Since the lattice parameter of Ge (5.657 Å) is intermediate between those of Si (5.43 Å) and α-Sn (6.49 Å), $Si_{1-x-y}Ge_xSn_y$ materials containing a suitable level of Sn could lattice match Ge, thereby allowing epitaxial growth of Ge/Sn_xGe_{1-x} heterostructures

and related photonic devices based solely on group IV materials.[8] Moreover, this ternary system offers the potential of band gap engineering and tuning of the optical properties, as indicated by theoretical studies conducted by Soref and Perry.[9] We have recently computed the properties of strained Ge layers grown on relaxed $Si_{1-x-y}Ge_xSn_y$ layers and we find that for appropriately selected Si/Sn ratios the heterostructure is a direct gap Type I system with both electrons and holes confined in the pure Ge layers. This remarkable prediction warrants an intensive program to develop Si-Ge-Sn alloys.

Our synthetic strategy for preparation of Si-Ge-Sn structures is focused on UHV-CVD reactions of the gaseous compound SiH_3GeH_3 with SnD_4. The former is a simple derivative of GeH_3GeH_3 in which one of the GeH_3 groups is replaced with SiH_3 thus forming a molecular core with direct Si-Ge bonds. H_3SiGeH_3 is a stable, gaseous compound and it is synthesized by using a new and high yield method outlined below.

$$CF_3SO_3SiH_3 + KGeH_3 \rightarrow H_3SiGeH_3 + KO_3SCF_3$$
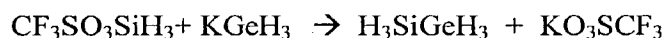
Prior to growing Si-Ge-Sn we performed controlled experiments involving the thermal dehydrogenation of H_3SiGeH_3 to study the deposition characteristics of this compound on Si(100) and thereby determine optimum conditions for growth of the target Si-Ge-Sn concentrations. We found that complete decomposition of H_3SiGeH_3 occurs readily at 450-700 °C to yield coherent SiGe quantum dots. Only partial decomposition takes place between 450 °C and 375°C to form amorphous hydrogenated films and no significant decomposition was obtained at 350 °C indicating that this temperature might be a reasonable starting point to initiate reactions of SiH_3GeH_3 and SnD_4 and produce Si-Ge-Sn films. Our previous studies have also indicated that 350 °C is also the optimum

3

temperature for incorporation of 2-6 at % Sn into tetrahedral Ge lattice sites without any phase segregation and Sn precipitation.

The growth of $Si_{1-x-y}Ge_xSn_y$ was initially investigated directly on Si (100). The reactions of H_3SiGeH_3 and SnD_4 at 350 °C produced layers (70-100 nm thick) of hydrogenated $Si_{1-x-y}Ge_xSn_y$ films, indicating that the presence of Sn increases the reactivity of the precursor and facilitates film growth via facile elimination of H_2 from the Si-H and Ge-H bonds. Since the films grown in this fashion were amorphous, we explored next the use of buffer layers of $Ge_{1-x}Sn_x$ (x=3-4 at. %) to induce crystallization and epitaxial film formation. We chose $Ge_{1-x}Sn_x$ alloys because they posses crystallographic, morphological and mechanical properties that make them uniquely suitable for use as templates on Si substrates. These materials grow as highly uniform, strain-free layers with smooth and continuous surface morphologies (typical AFM rms values are 0.5 and 1.4 nm) and display extremely low concentrations of threading defects, particularly those that extend to the uppermost surface (the quality of pure Ge films grown on Si by similar methods is much worse). In addition, they are high compressibility (softer) solids compared to either Si and $Si_{1-x-y}Ge_xSn_y$ and thereby can act as potential spacers that can conform structurally and readily absorb the differential strain imposed by the more rigid Si and Si-Ge-Sn.

The $Ge_{1-x}Sn_x$ buffer layers were grown on Si(100) via reactions of Ge_2H_6 and SnD_4 at 350 °C. The growth of the $Si_{1-x}Ge_xSn_y$ films was conducted immediately thereafter, *in situ*, via reactions of appropriate concentrations of SnD_4 and H_3SiGeH_3. Rutherford backscattering (RBS) in random mode was used to determine the bulk composition of the $Ge_{1-x}Sn_x/Si_{1-x-y}Ge_xSn_y$ heterostructures and to estimate the film thickness. RBS

4

channeling was used to determine the quality of the epitaxial growth and the degree of substitutionality of the elements in the structure. The RBS analyses showed that films with compositions ranging from $Si_{0.14}Ge_{0.84}Sn_{0.02}$ to $Si_{0.14}Ge_{0.80}Sn_{0.06}$ were grown on $Ge_{1-x}Sn_x$. The Sn content in the film was readily increased from 2 to 6 at. % in a controlled fashion by adjusting the partial pressure of gaseous SnD_4 in the reaction mixture. The Si incorporation remained constant, about 14 at. %, for all depositions conducted at 350 °C and was independent of the Sn concentration in the film. The RBS aligned spectra showed that Si, Ge and Sn channeled remarkably well despite the low temperature growth. The ratio between the aligned and random peak heights, which measures the degree of channeling of the incoming He ions, was identical for all three elements in a given sample. This indicates that Si, Ge and Sn occupy substitutional sites in the same diamond cubic structure and that the film is commensurate with the Si substrate. Figure 1 shows the RBS random and aligned spectra for the $Si_{0.14}Ge_{0.80}Sn_{0.06}/Ge_{0.96}Sn_{0.04}/Si$ heterostructure. Note that the Sn signal of the entire layer consists of two peaks, a narrow high energy peak corresponding to the epilayer and the adjoining low energy Sn peak of the buffer layer. The Sn concentrations in each layer as determined from the peak height are 6 and 4 at % respectively. The epilayer and buffer layer thickness as determined from the peak width are 45 and 115 nm respectively. The small peak located next to the Si substrate signal is due to the Si in the epilayer. The Si peak is well separated from the substrate signal (does not appear as a shoulder, or step adjacent to the substrate) indicating the absence of Si in the buffer layer.

The structural properties of the films were investigated by X-ray diffraction and high-resolution cross-sectional electron microscopy (XTEM). The x-ray data revealed

single-phase crystalline films, with no evidence of $Si_{1-x}Ge_x$, Si or Ge segregation. Rocking scans of the 004 reflections gave full width at half maxima between 0.25 and 0.50 degrees indicating a tightly aligned spread of the crystal mosaics. The unit cell parameter obtained from the (004) reflection for samples with 6 at. % Sn was 5.694 Å which is nearly identical to that of the underlying $Ge_{0.96}Sn_{0.04}$ buffer layer (5.70 Å). The 5.694 Å value is close to that predicted by Vegrads Law, which in this case assumes a linear interpolation between the lattice constants of elemental Si and $Ge_{1-x}Sn_x$ where x is the Sn content in the sample. Figure 2 shows the x-ray spectrum of a sample with composition $Si_{0.14}Ge_{0.84}Sn_{0.02}$ grown on Si(100) via a $Ge_{0.97}Sn_{0.03}$ buffer layer. The 004 reflections give lattice parameters of 5.644 Å for the $Si_{0.14}Ge_{0.84}Sn_{0.02}$ layer and 5.696 Å for the buffer layer. The 5.644 Å value is very close to that of Ge (5.657 Å) indicating that we have synthesized a ternary alloy that nearly lattice matches elemental Ge.

The XTEM studies revealed thick single crystal films with remarkably low concentrations of threading defects. Electron micrographs demonstrating high quality heteroepitaxial growth of a $Si_{0.14}Ge_{0.84}Sn_{0.02}$ sample on a $Ge_{0.97}Sn_{0.03}$ buffer layer are shown in Figure 3. A typical image of the Si(100) /$Ge_{0.97}Sn_{0.03}$ interface region shows the presence of occasional twins and {111} stacking faults which seem to annihilate above the interface. The main defects accommodating the large misfit between the two materials are Lomer edge dislocations, which are parallel to the interface plane. Finally the film surfaces are very smooth at the atomic scale. Atomic force microscopy (AFM) shows a typical root means square (rms) roughness of 0.6 to 1.5 nm. The XTEM images show that all layers are uniform in thickness and confirm smooth and continuous surface morphologies (Figure 4). The elemental uniformity across the entire layer was

6

investigated with energy dispersive x-ray (EDX) and electron energy loss (EELS) spectroscopies with nanometer sized electron probes. The nanospectroscopies showed a homogeneous distribution of Ge and Sn throughout the buffer layer, which is consistent with single-phase material. Analysis across the epilayer revealed significant concentrations of Si, and Sn and a large concentration of Ge. The constituent elements appeared together at every nanometer scale region probed without any indication of phase segregation or Sn precipitation. A typical compositional profile derived from EDX line scans showing a constant Si distribution across the epilayer is presented in Figure 4.

The local bonding environment of the Si-Ge-Sn alloys was characterized by Raman spectroscopy. Figure 5 shows the Raman spectrum of a $Si_{0.14}Sn_{0.06}Ge_{0.80}$ sample. The spectrum is reminiscent to that of Si_xGe_{1-x} alloys, with three main features that are known in the literature as the "Ge-Ge", "Si-Ge" and "Si-Si" peaks. The similarity with Si_xGe_{1-x} alloys shows that the incorporation of Sn does not alter the relative distribution of Si and Ge atoms in the lattice. No Sn-related vibrations are obvious in the spectra, presumably due to the low Sn-concentration. However, the presence of substitutional Sn is apparent from the measured frequencies of the Raman modes. The dotted lines in Figure 5 show the expected position[10] of the three main features in $Si_{0.14}Ge_{0.86}$ alloys. Our measured values are clearly downshifted with respect to the dotted lines, and we can show that this is due to the lattice expansion induced by Sn. Let us consider, for example, the Si-Si "mode". In Si_xGe_{1-x} alloys, its frequency is given by $\omega_{Si-Si} = 521 - 68x$.[10] It has been shown that this can be written as:[11]

$$\omega_{Si-Si} = 521 - 49x - 455\,\Delta a/a. \qquad (1)$$

7

The second term in Eq. (1) represents the mass disorder contribution, and the third term accounts for the stretching of the Si-Si bond in Si_xGe_{1-x} alloys.[12] Here Δa is the difference between the lattice constant of the alloy and that of Si. Since Ge atoms have very small displacements for Si-Si modes, we assume that their substitution for even heavier Sn atoms does not have any effect on the first term of Eq. (1). Hence the difference between the measured Si-Si frequency and the corresponding dotted line originates entirely from the second term in Eq. (1). If we imagine substituting 6% Ge with 6% Sn, the additional expansion of the lattice is 0.073 Å, which leads to an additional frequency shift of -7 cm^{-1}. This is in very reasonable agreement with the experimental value of -9 cm^{-1}, particularly in view of the approximations made and the fact that Eq. (1) is most accurate for Si-rich alloys.

In summary, a wide range of spectroscopic and microscopic data show that we have created, device quality single-phase $Si_{1-x-y}Ge_xSn_y$ alloys with metastable concentrations and structures on Si(100) (the thermodynamic solubility limit of Sn in $Si_{1-x}Ge_x$ is less than 0.5 at.%). The combination of template mediated growth, involving compliant $Ge_{1-x}Sn_x$ buffer layers, and a unique reaction pathway, based on specifically designed interactions of simple hydrides at low temperatures, produces materials that cannot be obtained by conventional methods.

References

1. D. W. Jenkins and J. D. Dow, Phys. Rev. B **36**, 7994 (1987).

2. K. A. Mader, A. Baldereschi, and H. von Kanel, Solid State Commun. **69**, 1123 (1989).

3. O. Gurdal, R. Desjardins, J. R. A. Carlsson, N. Taylor, H. H. Radamson, J. E. Sundgren, and J. E. Greene, Appl. Phys. Lett. **67**, 956 (1995).

4. P. R. Pukite, A. Harwit, and S. S. Iyer, Appl. Phys. Lett. **54**, 2142 (1989).

5. G. He and H. A. Atwater, Phys. Rev. Lett. **79**, 1937 (1997).

6. M. Bauer, J. Taraci, J. Tolle, A. V. G. Chizmeshya, S.Zollner, D. J. Smith, J. Menendez, C. Hu, and J. Kouvetakis, App. Phys. Lett. **81**, 2992 (2002).

7. Matthew Bauer, A.V.G. Chizmeshya, D.J. Smith, Jose Menendez and J. Kouvetakis *submitted to Phys. Rev. Lett.*

8. R. A. Soref and L. Friedman, Superlattices and Microstructures **14**, 189 (1993).

9. R. A. Soref and C. H. Perry, J. Appl. Phys. **69**, 539 (1991).

10. H.K. Shin, D.J. Lockwood, J.-M. Baribeau, Solid State Commun. **114**, 505 (2000)

11. M. Meléndez-Lira, J. D. Lorentzen, J. Menéndez, W. Windl, N. Cave, R. Liu, J. W. Christiansen, N. D. Theodore, and J. J. Candelaria, Phys. Rev. B **54**, 12866 (1997).

12. J. Menéndez, in Raman Scattering in Materials Science, edited by W. H. Weber and R. Merlin (Springer, Berlin, 2000), Vol. 42, p. 55.
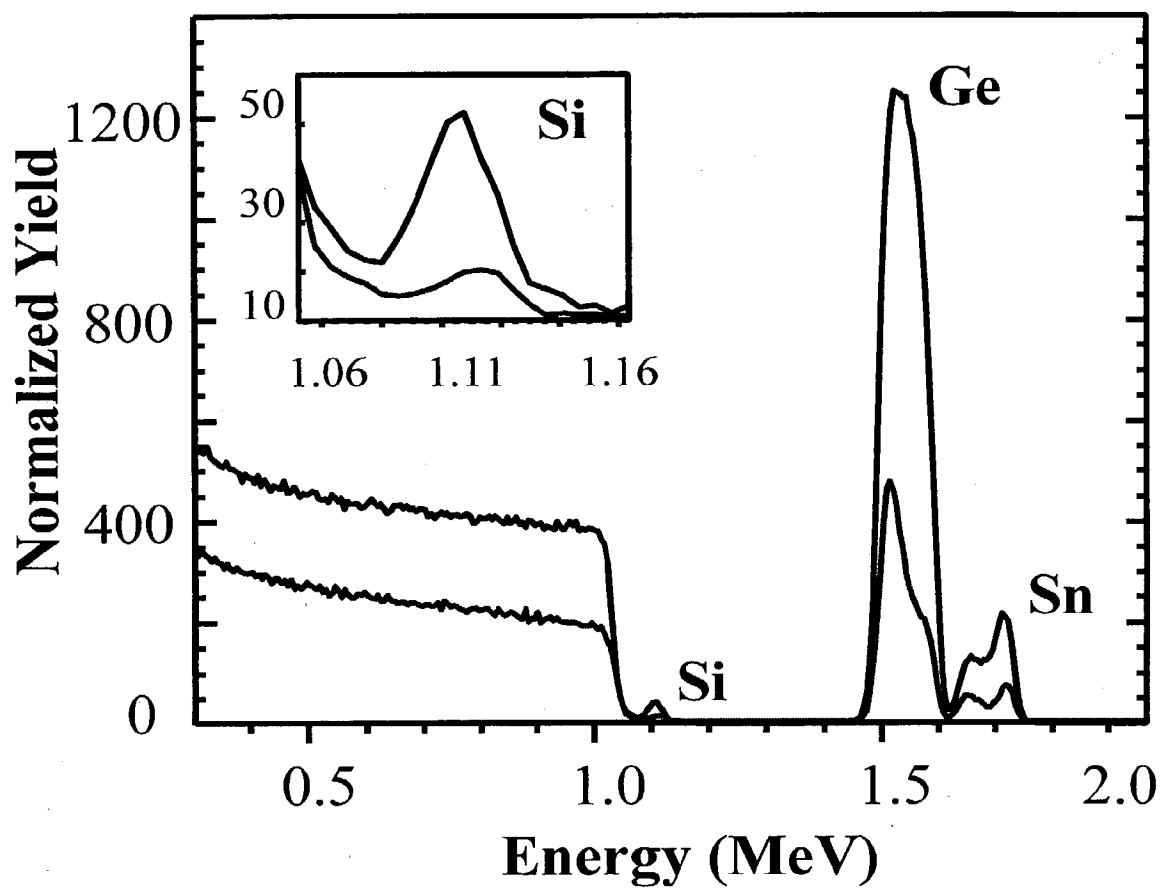
Figure 1 (Bauer et al.)
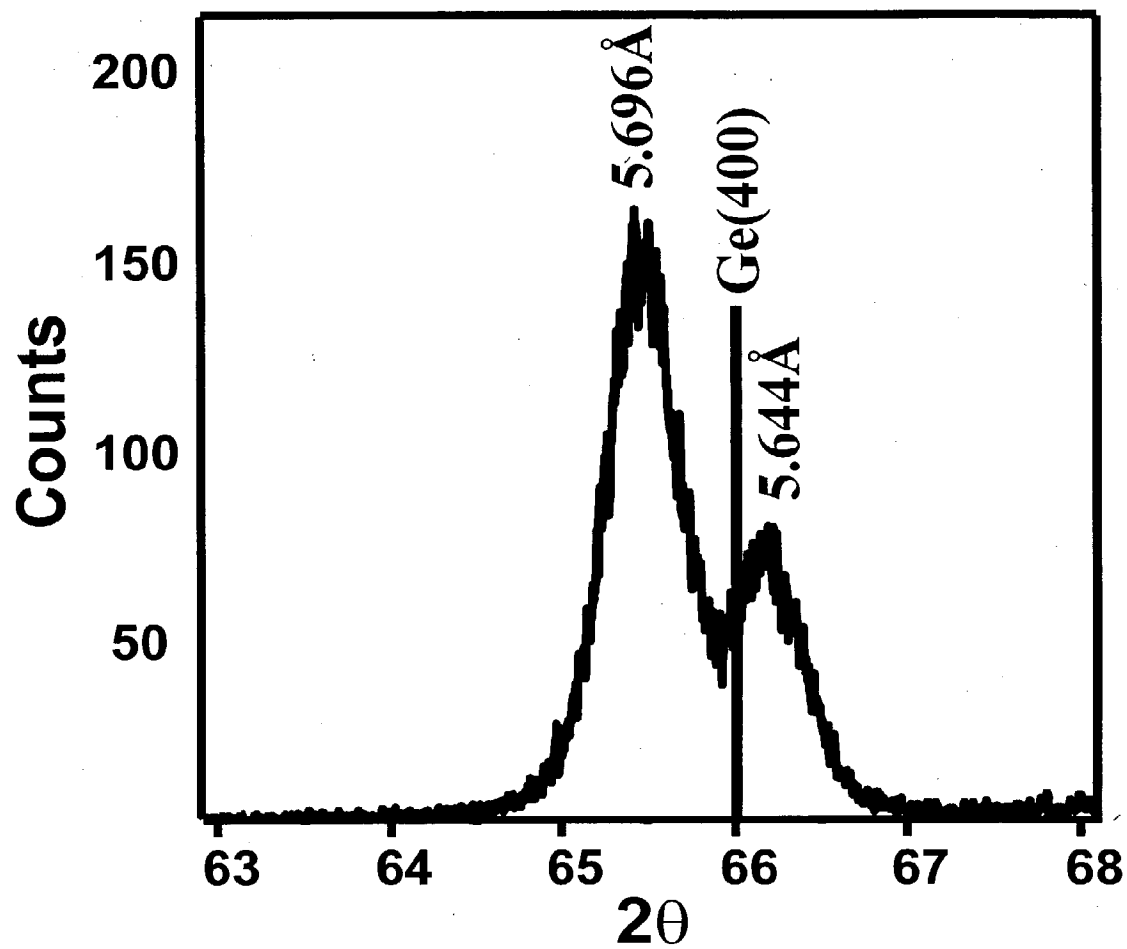
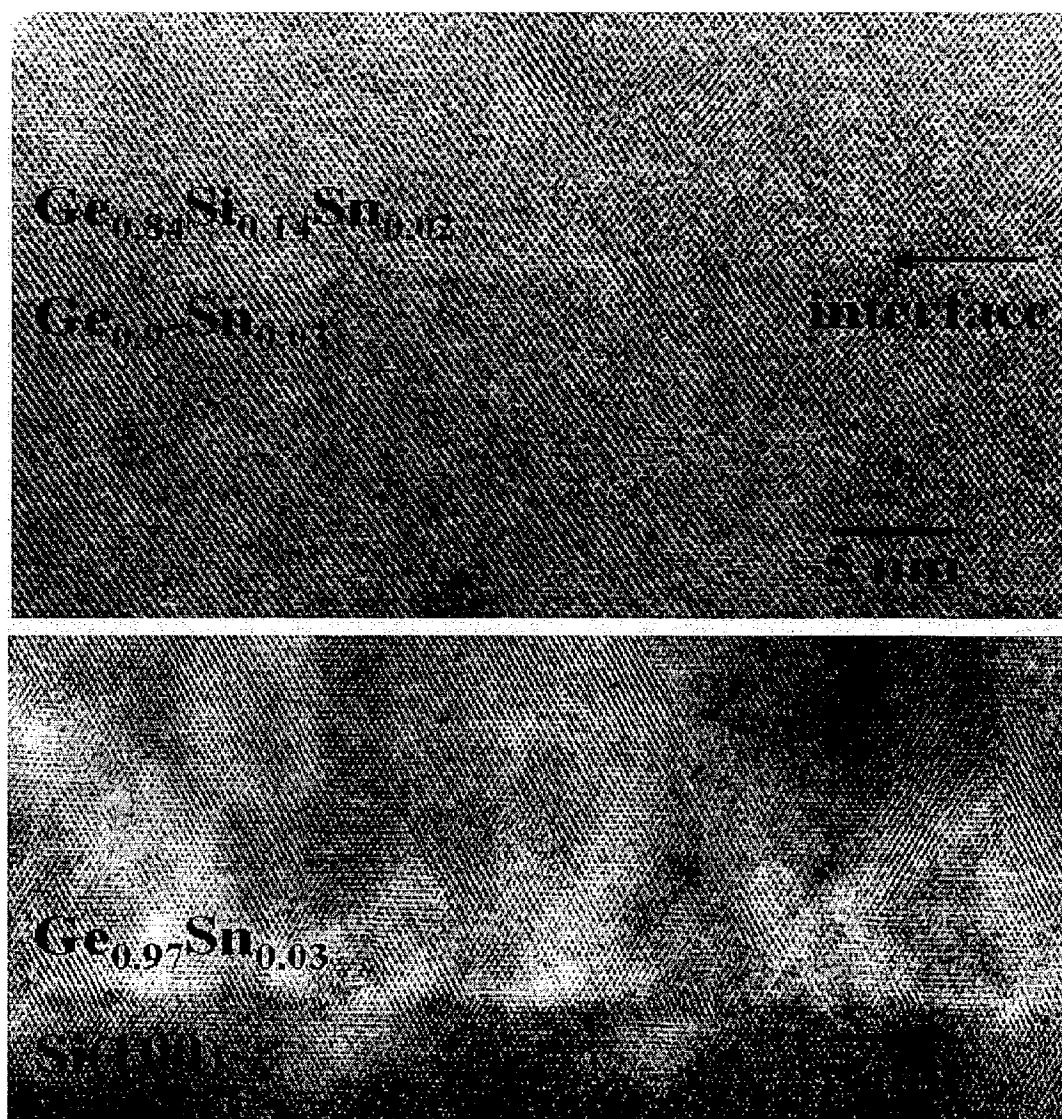*Figure 2 (Bauer et al.)*

Figure 3 (Bauer et al.)
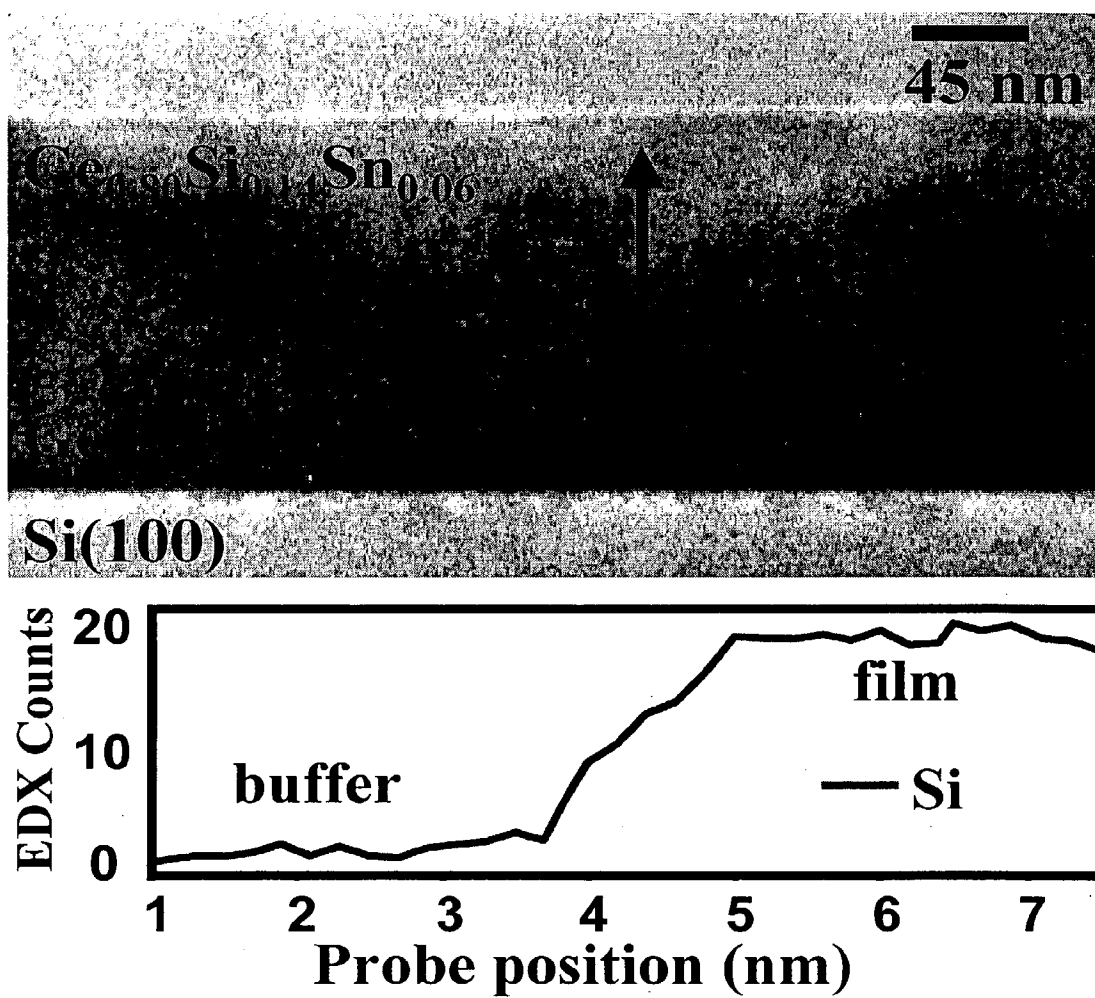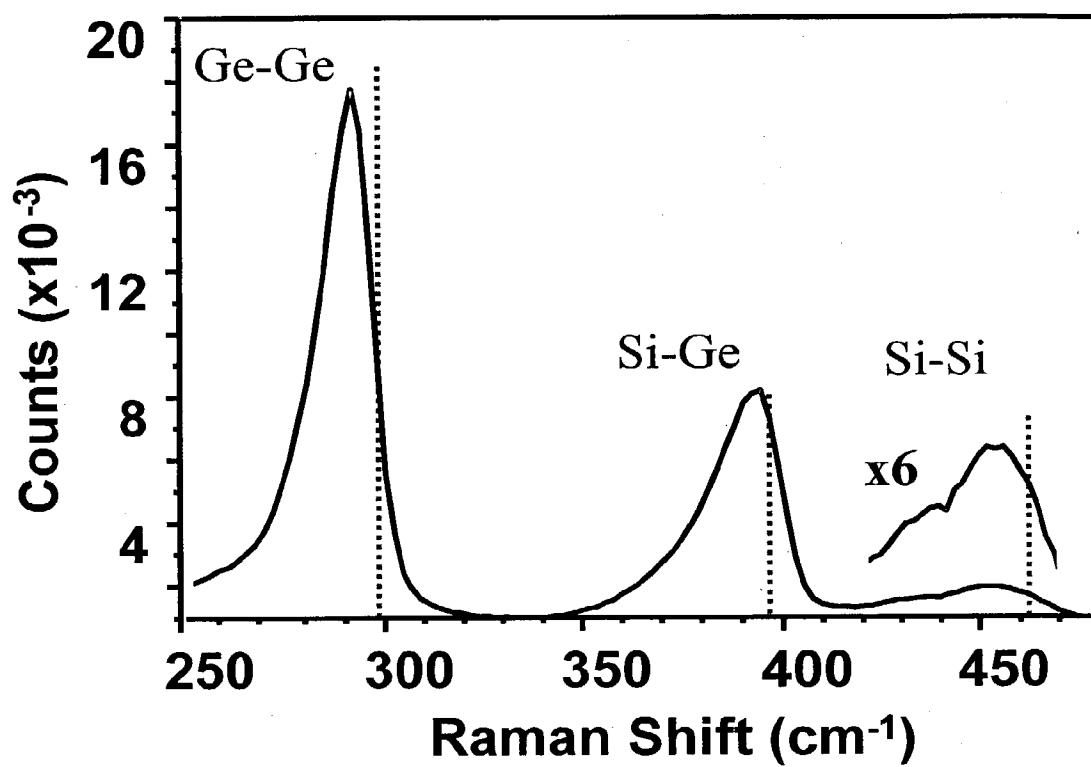
Figure 4 (Bauer et al.)

Figure 5 (Bauer et al.)

Figures

Figure 1. RBS random and channeled spectra of $Si_{0.14}Ge_{0.80}Sn_{0.06}$ epilayer and $Ge_{0.96}Sn_{0.04}$ buffer layer showing a highly aligned and epitaxial alloy heterostructure. Inset shows an enlarged view of the Si peak which channels remarkably well indicating complete substitutionality of the Si atoms in Si-Ge-Sn lattice.

Figure 2. X-ray diffraction pattern (θ -2θ scan) for the $Si_{0.14}Ge_{0.84}Sn_{0.02}/Ge_{0.97}Sn_{0.03}$ heterostructure grown on Si(100). The higher intensity peak with d = 5.696 Å corresponds to the 004 reflection of the buffer layer. The peak with d = 5.644 Å is 004 reflection of the $Si_{0.15}Ge_{0.83}Sn_{0.02}$ overlayer. The dark line shows the location of the corresponding peak of pure Ge for comparison.

Figure 3. High-resolution electron micrographs of $Si_{0.14}Ge_{0.84}Sn_{0.02}$. Top panel shows the $Si_{0.14}Ge_{0.84}Sn_{0.02}/Ge_{0.97}Sn_{0.03}$ interface demonstrating virtually perfect and defect-free heteroepitaxial character. Bottom panel shows the $Si/Ge_{0.97}Sn_{0.03}$ interface. Lomer edge dislocations are located at the interface and common defects such as stacking faults and twins are visible above interface.

Figure 4. Top panel is a cross sectional electron micrograph of the entire $Si_{0.14}Ge_{0.80}Sn_{0.06}/Ge_{0.96}Sn_{0.04}/Si$ heterostructure showing exceptional uniformity of the film thickness. The thickness of the buffer layer and the $Si_{0.14}Ge_{0.80}Sn_{0.06}$ epilayer are 115 nm and 45 nm respectively, which are close to the values obtained from the RBS spectra

15

(see Figure 1). Bottom panel shows the EDX profile of Si across the buffer layer/epilayer interface. The slope at the interface is attributed to Si fluorescence by Ge.

Figure 5 Raman spectrum of a $Si_{0.14}Ge_{0.80}Sn_{0.06}$ film showing the Si-Si, Si-Ge and Ge-Ge peaks at 454 cm^{-1}, 393 cm^{-1} and 292 cm^{-1} respectively. The dotted lines represent the expected peak positions for a relaxed film where all the Sn atoms are replaced by Ge atoms (the values for Si-Si, Si-Ge and Ge-Ge are 462 cm^{-1}, 396 cm^{-1} and 298 cm^{-1} respectively).

New and Practical Procedures for Development of $Ge_{1-x-y}Sn_xE_y$ (E=P,As,Sb) and Related Semiconductor Alloys

1. Novel molecular hydrides for dopant applications in the Si-Ge-Sn semiconductor system.

Overview

Development of methods dealing with incorporation of group V atoms such as P, As and Sb into Ge-Sn materials and other group IV semiconductors is described. These atoms are commonly utilized as dopants in the activation of industrially applied semiconductor materials such as Si, Si-Ge, and Ge. The focus of this report is to describe detailed new synthetic strategies based on novel molecular hydride sources to incorporate these atoms into the diamond lattice of these semiconductor systems. These sources are the previously known trigermylphosphine $P(GeH_3)_3$, trigermylarsine $As(GeH_3)_3$, and trigermylstibine $Sb(GeH_3)_3$ family of compounds. We are pursuing a comprehensive development because of potential applications in low temperature, low cost, high efficiency doping processes that are conducted via simple, single-step techniques. These compounds are particularly designed to serve as dopant sources for the newly developed and extremely promising Ge-Sn and Si-Ge-Sn systems so that these materials can are utilized to produce useful devices. Ion implantation methods and conventional CVD of the well known PH_3 and AsH_3 analogs require severe and often hostile processing conditions and are expected to be incompatible with the properties and stability range of the relatively fragile Ge-Sn lattice. In addition PH_3 and AsH_3 are highly toxic and in fact can be lethal in relatively small doses, whereas the trigermyl family of compounds are safer and also easier to handle and store.

Appendix D

1

We expect to use $P(GeH_3)_3$, $As(GeH_3)_3$, and $Sb(GeH_3)_3$ to dope functional materials such as SiGe, SiGeC, Ge and Si at levels that cannot be achieved by conventional methods. Highly doped concentration of these semiconductors that could be obtained via this route will have crucial advantages in electronic and optical (IR) device design, performance and fabrication. Currently Si-based semiconductors are doped with As or P by ion implantation but there are limits as to how much dopant can be introduced into the structure. We expect to increase the free carrier concentration by using these precursors with direct Ge-P, As, Sb bonds and atomic arrangements that are structurally compatible with the Ge-Sn lattice. Other applications of these compounds will include formation of super doped Si-Ge, Ge and related narrow band gap semiconductors by CVD reactions. The objective is to increase the density of states and produce a true covalent metal with interesting superconductive properties. Covalent metals such as the recently discovered superconductive magnesium diboride are rare. The potential to open up new classes of similar covalent metals via the current precursor method could be compelling and high risk high pay off goal this project. Such materials have the potential for both applications in metal-semiconductor contacts and depending on the density of states achievable ground breaking superconducting properties. Furthermore the atomic constituents of of the Ge-Sn:As materials, in particular, might assume alternative structural arrangements with novel elastic properties.

Several previous reports provide only preliminary results of the synthesis and some basic physical properties of these $P(GeH_3)_3$, $As(GeH_3)_3$, and $Sb(GeH_3)_3$ compounds. Unfortunately the original syntheses are conducted by procedures that provide low yields (in certain cases only traces of the desired product are produced) and are exceedingly

2

difficult and involve steps that can be potentially dangerous especially for the scaling up phase to produce industrial-scale quantities of the product. Our work demonstrates new and practical methods to prepare, isolate, purify and handle these molecules in sufficient quantities to make them useful as chemical reagents as well as CVD gas sources.

Introduction

The successful synthesis of random alloys and stoichiometric compounds in the GeSn system has prompted investigations to develop new methods to dope thin films of these new materials with donor and acceptor elements such as B, P, As and Sb etc . The objective is to incorporate appropriate concentrations of activated atoms into the Ge-Sn lattice and determine the electrical and transport properties as a function of concentration. The dopant atoms are introduced into the host lattice in situ, during film growth via low temperature chemical reactions of specially designed molecular precursors. These compounds are designed to be stable and volatile at room temperature and posses the necessary reactivity to dissociate completely at Ge-Sn growth conditions, via elimination of benign and stable byproducts that do not contaminate the film. The ideal byproduct in this case is the H_2 molecule indicating that the precursors must be carbon-free inorganic hydrides that incorporate the desired elements P, As and Sb within a Ge coordination environment. The candidate precursors that fulfill the above requirements are the trigermylphosphine $P(GeH_3)_3$, trigermylarsine $As(GeH_3)_3$, and trigermylstibine $Sb(GeH_3)_3$ family of compounds. The reactions of these molecules with appropriate concentrations of SnD_4 and/or $(GeH_3)_2$ will generate Ge-Sn compositions doped with the desired levels of a group V element. Typically n-doping is performed by use of

3

molecular PH_3 and AsH_3 (the SbH_3 analog is unstable) or by ion implantation using solid sources of the elements. Ion implantation has advantages such as relatively low processing temperatures and the short processing times. However, it also has some major disadvantages, such as significant substrate damage and composition gradients across the film. For the thermodynamically unstable Sn-Ge lattice the re-growth temperatures, that are required to repair the implantation damage of the crystal, may exceed the temperature stability range of the film, resulting in phase segregation and precipitation of Sn. Therefore, the molecular source approach is likely to be more appropriate than the implantation route since the introduction of the dopant takes place in situ during growth and as the lattice is generated. In a typical growth process conducted by either gas-source molecular beam epitaxy (GS-MBE) or chemical vapor deposition (CVD), a compound with the general formula $E(GeH_3)_3$ (E = P, As, or Sb) compound will co-deposited along with the host Ge-Sn material. This growth reactions will eliminate hydrogen and generate in situ the Ge_3E molecular core, which contains the dopant atom surrounded by three Ge atoms. This arrangement represents a simple compositional and structural building block of the host lattice. The use Ge_3E core as building block will also completely exclude formation of undesirable E-E bonding arrangements that may lead to clustering or segregation of the E dopant species. Thus the new approach is most likely to yield a highly homogeneous random distribution of the dopant at distinct atomic sites throughout the film. Furthermore, the doping levels may be precisely controlled by careful adjustment of the flux rate of the precursor during the course of the layer growth. A crucial benefit of trigermylarsine is its lower thermal stability compared to AsH_3,

4

which is likely to allow much lower depositions temperatures than those obtained in conventional CVD utilizing sources such as AsH_3 and related hydrides of phosphorus.

Synthetic methods

There is an extensive body of published work dealing with synthesis, properties and reactions of the compounds $(Me_3Si)_3E$, $(Me_3Ge)_3E$, $(Me_3Sn)_3E$, and $(Me_3Pb)_3E$ (E = P, As or Sb)[1-20], which are the organometallic analogs of the desired precursors. These materials have been widely utilized as common reagents in classical metathesis reactions to produce large families of molecular systems that incorporate the $(Me_3Si)_2E$, $(Me_3Ge)_2E$, and $(Me_3Sn)_2E$ ligands. However there is relatively little activity associated with the corresponding hydrides, which are completely C-H free, despite their potential importance as precursors for deposition of novel microelectronic and oproelectronic materials. The $(SiH_3)_3E$ family of molecules has been synthesized [21-26] and the properties have been investigated. The high reactivity of the Si-H bonds and the absence of carbon from the molecular architecture indicate that these compounds could be ideal sources for low temperature depositions of semiconductors doped with P and As. The synthetic methods are nevertheless complex and require use and handling of highly toxic, explosive and pyrophoric reagents such as PH_3, AsH_3, KPH_2 etc. In additon, the reaction yields are too low to even be considered useful for routine laboratory use. Thus these compounds could not be viable sources for industrial applications.

On the other hand there very few reports concerning the germanium analogs $(GeH_3)_3E$,[27-30] and no report has been found describing the tin $(SnH_3)_3Sn$ and lead $(PbH_3)_3Pb$ species. The $(GeH_3)_3P$, $(GeH_3)_3As$, $(GeH_3)_3Sb$ are desirable for the synthesis

5

of $Ge_{1-x-y}Sn_xP(As,Sb)_y$ systems. $(GeH_3)_3P$ was originally obtained by treating a small excess of GeH_3Br with $(SiH_3)_3P$ as illustrated by the equation below.

$$3\ GeH_3Br + (SiH_3)_3P \rightarrow 3\ SiH_3Br + (GeH_3)_3P$$

No yield was reported and the product was characterized by hydrogen analysis, ^{1}H and ^{31}P NMR, IR and mass spectroscopy. $(GeH_3)_3P$ was described as a colorless liquid with a melting point of -83.8^oC and a vapor pressure of 1 mmHg at 0^oC.

$(GeH_3)_3As$ and $(GeH_3)_3Sb$ were prepared in low yields by the reaction of bromogermane with the corresponding silyl compounds (which as indicated above are difficult to produce in sufficient yields to be practical reagents for routine laboratory synthesis). These compounds were identified and characterized by NMR, IR, and Raman spectroscopies. These molecules were found to decompose very slowly, over time, at room temperature to give germane and an unidentified involatile substance. Their vapor pressures were not reported but there was mention of distilling the liquids onto CsBr plates to obtain IR spectra, indicating that they are sufficiently volatile to allow significant mass transfer under vacuum.

$(GeH_3)_3P$ has also been synthesized by the redistribution reaction of silylphosphines and germylphosphines in the presence of B_5H_9.[31] In these reactions, B_5H_9 and GeH_3PH_2 were intermixed in the gas phase at room temperature and the trigermylphosphine (20% yield) was found in the reaction vessel along with PH_3, GeH_4, and unreacted starting material. We have discovered a new convenient and high yield method to prepare $(GeH_3)_3P$, $(GeH_3)_3As$, and $(GeH_3)_3Sb$. This new route is based on the general reaction described by the equation below, and provides large concentrations of the final product (>70 %) to allow a thorough characterization, purification and ultimately applications in film growth.

This new procedure is extremely simple and utilizes the more common and relatively inexpensive trimethylsilyl derivatives $[(CH_3)_3Si)]_3P$, $[(CH_3)_3Si)]_3As$, and $[(CH_3)_3Si)]_3Sb$ for which straightforward, large scale syntheses are well established.

$$3 \; GeH_3Br + [(CH_3)_3Si)]_3E \rightarrow 3 \; (CH_3)_3Si \; Br + (GeH_3)_3E \quad (E = P, As, Sb)$$
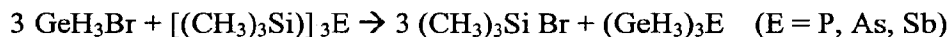
The preparation is achieved by the reaction of GeH_3Br with $[(CH_3)_3Si)]_3E$ (the former is readily obtained by a single step reaction of GeH_4 with Br_2). The $(GeH_3)_3E$ products are obtained as colorless volatile liquids (consistent with previous reports) and are purified by trap-to-trap fractionation. Typical yields ranging from 70% to 76% are obtained. The ^1H NMR and gas phase IR data of our products closely match the previously reported values. These data conclusively reveal that we are able to synthesize and purify the desired compounds. Their application in CVD was also examined by a brief survey of growth experiments.

Depositions of trigermylarsine *via* ultra-high vacuum CVD (UHV-CVD) showed that the molecule decomposes on Si (100) at temperatures as low as 350°C to form a thin films with approximately 30 at.% As indicating that the entire Ge_3As molecular core is incorporated into the deposited material. Low-pressure CVD growth of As doped $Ge_{1-x}Sn_x$ films was also demonstrated. Arsenic concentrations up to 2 at % were obtained. Doping level incorporations were also achieved by reactions of appropriate concentrations of $As(GeH_3)_3$. Overall, the growth experiments demonstrated that compositional control of As in Ge-Sn can be obtained by simply varying the partial pressure of the reactant gases $As(GeH_3)_3$, SnD_4 and Ge_2H_6. The films have been characterized by RBS to determine the Ge to Sn ratio, particle induced X-ray emission (PIXE) to determine the As concentrations **see Figure 1**, TEM to show that the

7

microstructure and epitaxial character is of good **(Figure 2)** quality. and x-ray diffraction to show that the film has an average diamond cubic lattice. Low energy secondary ion mass spectroscopy (SIMS) showed highly homogeneous profiles of As and the Ge and Sn constituent elements throughout the film **(Figure 3).**

2. Synthesis of superconductive Si-Ge: P, As, Sb

The superconducting transition temperature predicted by standard BCS theory is approximately given by[31]

$$T_c = 1.14 \frac{\hbar \omega_D}{k_B} e^{-1/VD(\mu)}, \tag{1}$$

where ω_D is Debye's temperature, V the average electron-phonon coupling, and $D(\mu)$ the electronic density of states at the Fermi level. One notices from Eq. (1) that an increase in the density of states leads to an increase in the transition temperature, and that this dependence is very strong because the density of states appears in the exponential factor.

Doped semiconductors are in principle metallic systems susceptible of semiconducting transitions, but they are not usually viewed as potential superconducting materials. This is due to the relatively low electron concentrations achievable by conventional doping and to the low density of states near the bottom of the conduction bands in most standard semiconductors. Nevertheless, some theoretical and experimental effort has been devoted to the study of possible superconductivity in these systems. In particular, Cohen speculated[32] that a superconducting transition could be made observable in $Si_{1-x}Ge_x$ alloys by carefully tuning the concentration x so that the

8

conduction band has 12 minima of equal energy along the {111} and {100} directions in the Brillouin zone.

Our doping approach will involve CVD reactions of $P(GeH_3)_3$, $As(GeH_3)_3$, and $Sb(GeH_3)_3$ with the appropriate Si and Ge hydrides. It has the potential of leading to much higher dopant concentrations, and therefore the issue of superconductivity in semiconductor system may acquire an entirely new relevance. Moreover, at the time the Cohen paper was written the only practical way to tune a band structure was by alloying. By contrast, today we control two additional band tuning mechanisms: epitaxial strain and confinement. By growing thin layers of doped semiconductors on appropriate substrates we can achieve much higher density of states than by simple alloying. This may lead to substantial increases in the superconducting transition temperatures of these materials.

Development $H_3Si-GeH_3$. A new volatile hydride precursor to SiGe epilayers and nanostructures and a superior alternative to GeH_4 in CVD of $Si_{1-x}Ge_x$ processes.

The most common gas sources for CVD of Si-Ge semiconductors are the classical hydrides SiH_4 and GeH_4. Both are synthesized using conventional methods and can be processed to obtain semiconductor grade specifications and purities. A high yield method of synthesis for GeH_4 was recently developed by Voltaix Corporation. A hybrid of GeH_4 and SiH_4 with molecular formula $H_3Si-GeH_3$ is of enormous technological interest because of its potential application as a single, low-temperature precursor to grow high Ge content $Si_{1-x}Ge_x$ alloys. This compound can be adapted easily to existing CVD technologies and it is expected to become the ideal alternative to GeH4 and provide additional benefits such as low processing temperatures, stoichiomtery control of the

9

film, and homogeneous compositional distributions of the Si and Ge elements. This material can also be used to grow stoichiometric SiGe via a unimolecular dehydrogenation as well as alloys with concentrations x < 0.50 via CVD reaction of SiH_4 or Si_2H_6. The original synthesis of $H_3Si\text{-}GeH_3$ was reported by McDiarmad et al. in 1964. These authors used electric discharges of silane and germane to obtain small quantities (5% yield) of the product. The primary goal was to establish the identity of the compound and study key physical and spectroscopic properties. Recently we discovered a new and practical method to prepare the compound in practical yields (30 %) so that it can be utilized in semiconductor research and development. Our method employees inexpensive reagents and conventional laboratory procedures that are much easier to those described in the previous synthesis. Our method has afforded excellent purity material which was used to produce SiGe nanostructures on Si(100) via the GSMBE method and novel Si-Ge-Sn alloys via UHV-CVD. The synthetic procedure is summarized by the equation below:

$$H_3SiO_3SCF_3 + KGeH_3 \rightarrow H_3SiGeH_3 + KSiO_3SCF_3$$
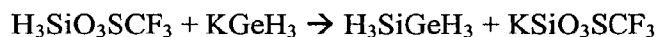
Procedure

A 45 mL solution of 4.00 g $KGeH_3$ (3.49 mmol) in monoglyme was slowly added dropwise, *via* addition funnel, over the course of 45 minutes to a 35 mL toluene solution of 9.43 g $H_3SiOSO_2CF_3$ (5.24 mmol) in a 250 mL flask at -60° C. A distillation assembly of a series of traps was connected to the apparatus. The reaction procedure involved dropwise addition of a $KGeH_3$/monoglyme solution to $H_3SiO_3SCF_3$ solution in monoglyme with vigorous stirring. The products were removed by continuous passing through U traps maintained at -78° and -196° C traps under static vacuum. This

10

procedure was maintained until all the reagents were combined and reacted. The -60° C bath was then removed and the reaction vessel was slowly warmed to room temperature with continuous pumping. Pumping was maintained for an additional hour at room temperature. The products was collected in the -196° C trap and the impurities remained in the -78° C trap. Gas-phase IR spectroscopy revealed the presence of benzene, monoglyme, toluene (-78° C trap), germylsilane, silane, and germane (-196° C trap B). The compound was redistilled through traps held at -78°, -135° and -196° C in which pure H_3GeSiH_3 (-135° C trap) was obtained. A quantity of 185 Litter-Torr; 30% yield was obtained based on $KGeH_3$ used.
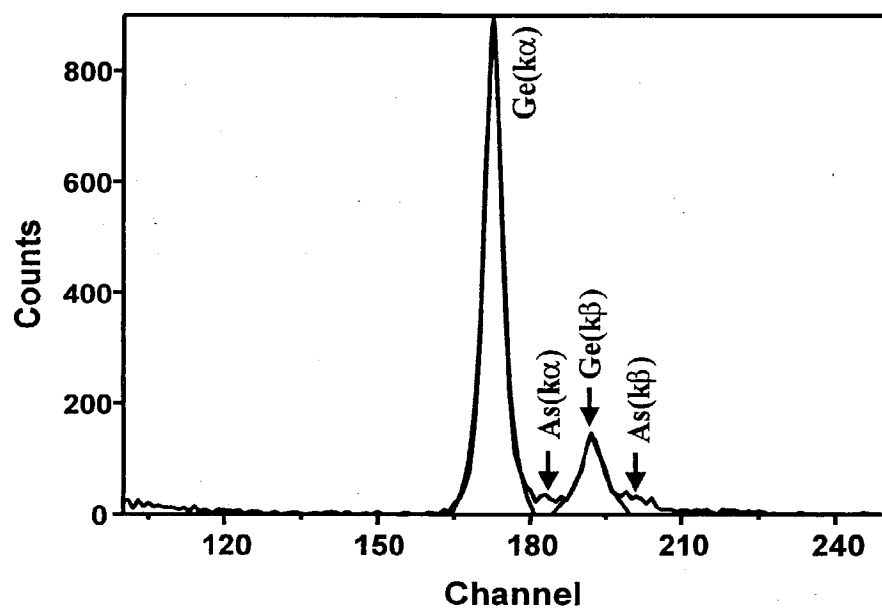
Figure 1. PIXE spectrum of Ge-Sn:As. Quantification obtained from fitting

the peaks showed that the film contained about 3% at % As.
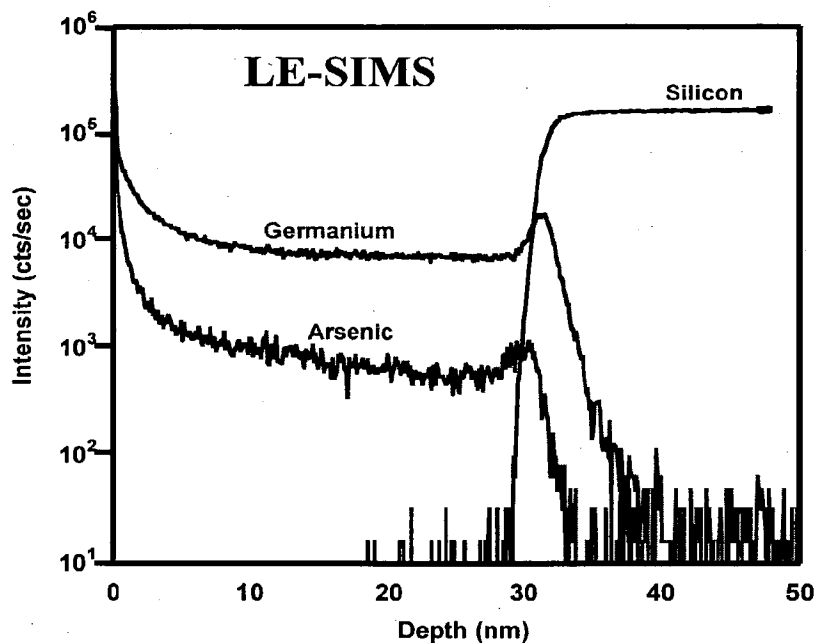
Figure 2. Low energy SIMS profile Ge-Sn:As, (3 at %As concentration) showing fairly homogeneous distribution of the elements
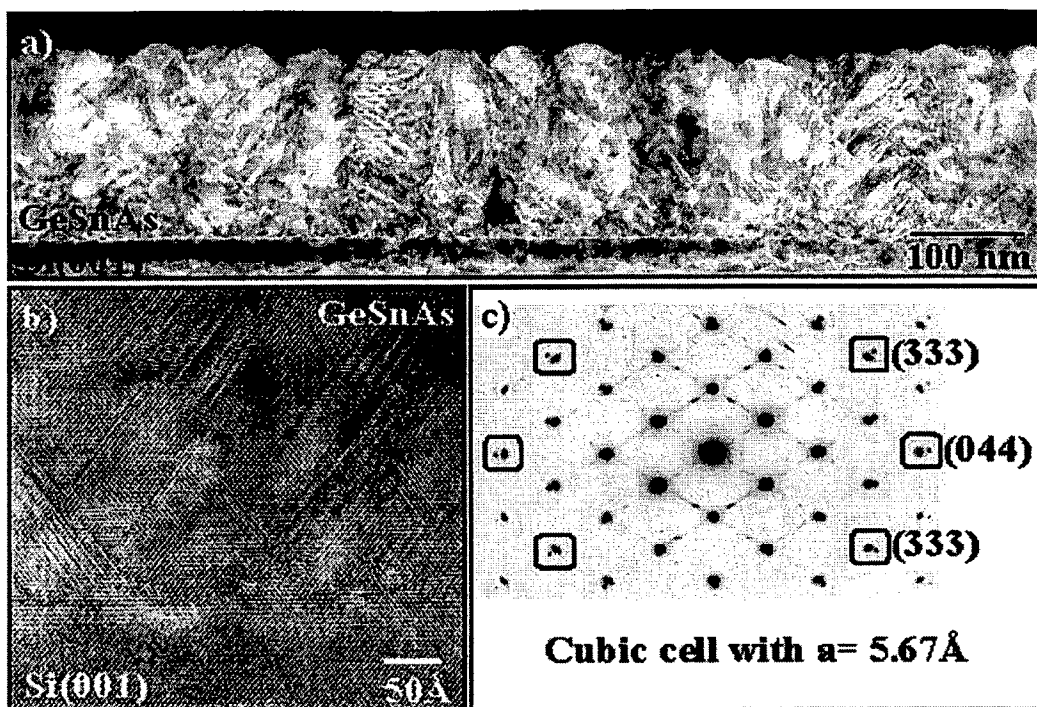
Figure 7.22. High resolution electron micrographs and diffraction pattern of Ge-Sn:As, (3 at %As). Top: Electron micrograph of the entire layer thickness,. Bottom (left) High resolution image of the Si/layer interface. Bottom (right): selected electron diffraction pattern of the interface region showing an average diamond cubic lattice.

References

1. G. A. Forsyth, D. W. H. Rankin, H. E. Robertson, *J. Mol. Struct.* **239**, 209, (1990)

2. H. Schumann, H. J. Kroth, *Z. Naturforsch., B: Anorg. Chem., Org. Chem.* **32B**, 523, (1977)

3. G. Becker, W. Hoelderich, *Chem. Ber.,* **108**, 2484, (1975)

4. H. Schumann, R. Fischer, *J. Organomet. Chem.* **88**, C13, (1975)

5. H. Schumann, L. Roesch, *J. Organometalic Chem.* **55**, 257 (1973)

6. H. Buerger, U. Goetze, W. Sawodny, *Spectrochi. Acta, Part A*, **26**, 671, (1970)

7. G. Becker, H. Freudenblum, O. Mundt, M. Reti, M. Sachs, *Synthetic Methods of Organometallic and Inorganic Chemistry*, **3**, 193, (1996)

8. S. Schulz, M. Nieger, *Journal of Organometalic Chemistry*, **570**, 275, (1998)

9. H. J. Breunig, M. Jonsson, R. Rosler, E. Lork, *Journal of Organometallic Chemistry*, **608**, (1981)

10. L. Roesch, W. Schmidt-Fritsche, *Z. Anorg. Allg. Chem*, **426**, 99, (1976)

11. H. Schumann, H. J. Kroth, L. Roesch, *Z. Naturforsch., Teil B*, **29**, 608, (1974)

12. H. Schmann, L. Roesch, *Chem. Ber.* **107**, 854, (1974)

13. A. V. G. Engelhardt, P. Reich, H. Schumann, *Z. Naturforsch., B: Anorg. Chem., Org. Chem., Biochem., Biophys., Biol.* **22**, 352, (1967)

14. D. Anderson, J. E. Drake, *Can. J. Chem.* **49**, 2524, (1971)

15. H. Schumann, U. Frank, W. W. Du Mont, F. Marschner, *J. Organomet. Chem*, **222**, 217, (1981)

16. M. Ates, H. J. Breunig, M. Denker, Phosphous, *Sulfur Silicon Relate. Elem.* **102**, 287, (1995)

17. E. Niecke, H. Westermann, *Anorg. Synthesis*, **4**, 330, (1988)

18. H. J. Breunig, V. Breunig-Lyriti, *Z. Naturforsch., B: Anorg. Chem., Org. Chem.* **34B**, 926, (1979)

19. H. J. Breunig, *Naturforsch., B: Anorg. Chem., Org. Chem.* **33B**, 244, (1978)

20. H. Schumann, A. Roth, O. Stelzer, M. Schmidt, *Inorg. Nucl. Chem. Lett.* **2**, 311, (1966)

21. G. Davidson, L. A. Woodward, E. A. V. Ebsworth, G. M. Sheldrick, *Spectrochim. Acta, Part A*, **23**, 2609, (1967)

22. B. Beagley, A. G. Robiette, G. M. Sheldrick, *Chem. Commun*, **12**, 601, (1967)

23. A. Blake, E. A. V. Ebsworth, S. G. D. Henderson, *Acta Crystallogr., Sect. C: Cryst. Struct. Commun*, **C47**, 489, (1991)

24. H. Siebert, J. Eints, *J. Mol. Struct.* **4**, 23, (1969)

25. D. C. McKean, *Spectrochim. Acta, Part A*, **24**, 1253, (1968)

26. J. E. Drake, J. Simpson, *J. Chem. Soc. A.* **5** 1039, (1968)

27. S. Cradock, E. A. V. Ebsorth, G. Davidson, L. A. Woodard, *J. Chem. Soc. A*, **8**, 1229, (1967)

28. D. W. H. Rankin, A. G. E. Robiet, G. M. Sheldrick, B Beagley, T. G. Hewit, *J. Inorg. Nucl. Chem.*, **31**, 2351, (1969)

29. E. A. V. Ebswort, D. J. Hutchison, J. Douglas, D. W. H. Rankin, *J. Chem. Res., Synop*, **12**, 393, (1980)

30. E. A. V. Ebsworth, D. W. H. Rankin, G. M. Sheldrick, *J. Chem. Soc. A*, **11**, 2828, (1968)

31. D. E. Wingeleth, A. D. Norman, *Phosphorus Sulfur*, **39**, 123, (1988)

32. P.L. Taylor and O. Heinonen, "A Quantum Approach to Condensed Matter Physics," Cambridge University Press, Cambridge, 2002, p. 250

33. M.L. Cohen, "Superconductivity in Many-Valley Semiconductors and in Semimetals," Phys. Rev. 134, A511-A521 (1964).

17